Chapter 1

Flexible Circuit Technologies for Biomedical Applications

Damien C. Rodger, Wen Li, James D. Weiland, Mark S. Humayun and Yu-Chong Tai

Additional information is available at the end of the chapter

http://dx.doi.org/10.5772/55308

1. Introduction

The human body is an incredibly complex organism that exhibits an impressive resilience to external influences, such as infecting bacteria and inhaled particles. This, however, proves to be a difficult problem to overcome when designing and implementing implantable devices for medical therapy, as the body is supremely primed to resist any artificial intervention. One of the critical parameters to consider is the mechanical compatibility of the implanted device with the tissue of interest. Additionally, the footprint of the device should ideally be as minimal as possible to decrease tissue damage and to minimize encapsulation responses. Until recently, however, it has proven difficult to integrate naturally inflexible solid state circuits with flexible components due to connection complexities and pitch limitations. In addition, material and fabrication limitations have prevented the implementation of thin-film cables, radiofrequency coils, and neural stimulation electrode arrays in implantable devices.

Here, after a brief review of the literature, we discuss novel flexible technologies being developed for biomedical applications, and especially for high density functional neural stimulation and recording. The distinctive parameters of a unique material, namely the semicrystalline thermoplastic parylene C, that make it particularly well-suited as a biocompatible substrate for thin-film biomedical circuits are discussed, explaining the reasoning for its use in a novel paradigm as a substrate and not just as a coating. In addition, we discuss a new packaging scheme that has been developed to enable high lead count interconnects using microfabrication equipment for alignment and patterning, and demonstrate a complete parylene-based stimulation microsystem combining radiofrequency coils with solid state circuits and electrodes in a parylene substrate. This integration of solid state circuits with flexible, biocompatible components gives rejuvenated hope for a new generation of neural

prosthetics aimed to provide eyesight to the blind and limb movement to para- and quadriplegic patients through spinal cord stimulation. These technologies can also enable integration of solid state devices with novel bioMEMS sensors in such a manner that devices previously only conceived of are now possible.

2. Outer retinal disease

Blindness due to such outer retinal diseases as retinitis pigmentosa (RP) and age-related macular degeneration (AMD) affect hundreds of thousands of people worldwide. In fact, it has been estimated by The Eye Diseases Prevalence Research Group and the National Eye Institute that AMD alone will affect three million people in the United States by the year 2020 [1]. In addition, the prevalence of RP has been estimated to be approximately 1 in 4000 [2]. Although the pathogeneses of these retinal photoreceptor diseases are, to date, not entirely understood, it is known that they are largely restricted to the outer retina, and that downstream circuitry, although it undergoes significant remodeling, is relatively spared [3-5]. There exist several possible approaches to thwarting the devastating effects of these diseases. Of these, the surgical, pharmacological, stem cell, and dietary approaches are promising. Laser ablation of leaky blood vessels and diets rich in antioxidants, for example, have been shown to slow the progress of AMD, but not to have any effect on its incidence. Effective pharmacologic agents, likewise, have long been elusive. Recent evidence has shown that stem cell therapy could also be a possibility for the treatment of such diseases, by possibly replacing the lost photoreceptors with stem cells capable of maturing into photoreceptors that then make connections with the rest of the retina [6]. However, such treatments, in reality, are still very far away from being used in clinical practice, and have a number of ethical and political barriers to their implementation.

In need of another possible treatment for these profound retinal diseases, in 1994 Humayun *et al.* reported the results of a pioneering study to electrically stimulate vertebrate retinas [7], a bioengineering approach that would possibly bypass the diseased photoreceptors in the visual pathway. In this study, bullfrog eyecups, as well as rabbit eyes (the rabbits were injected intravenously with sodium iodate, a chemical toxic to the retinal pigment epithelium and with other effects on photoreceptors), were stimulated with platinum electrodes. In their report, the following conclusion was made: "Surface electrical stimulation of the inner retina in normal eyes and in eyes with outer retinal degeneration can elicit a localized retinal response." This has since had a profound impact on the field of ophthalmology, by dramatically throwing an engineering solution into the mix of possible treatments for patients with devastating blindness due to outer retinal disease.

As a follow-up to this study, it was shown in 1996 by Humayun *et al.* that this seemingly simple approach of passing a carefully controlled electrical current through an electrode placed directly on the retinal surface to activate the still functional electrically excitable cells of the retina can also elicit visual percepts in humans with otherwise bare or no light-perception vision [8]. Perhaps even more important than the perception itself was the nature of the

perception. Subjects did not report seeing streaks or multiple percepts of light simultaneously when stimulating from one electrode, as might be expected if the axons of the ganglion cells, as they made their way to the optic nerve in the nerve fiber layer, were being stimulated. Instead, they reported seeing discrete, highly localized percepts that seemed to correlate very well with the location of stimulation. This suggested that it was not the axons that were the most electrically excitable, but instead the cell bodies of the several retinal ganglion cells (RGCs) or the bipolar, or even possibly amacrine or horizontal cells underlying the electrode. Indeed, it has since been conjectured that it could even be the characteristic right-angle bend in the axon of the RGCs that has maximal electrical excitability [9]. No matter the case, this was the confirmation of the feasibility of an engineering approach to treat human blindness with a "retinal prosthesis."

There are now a large variety of approaches to artificial vision, each with their own advantages and disadvantages. There is this epiretinal approach (Figure 1), in which an electrode array is placed directly on the retina from its anterior aspect. There is the subretinal approach, in which an electrode or photodiode array is placed within the layers of the retina [10], as is also shown in Figure 1 (this can be further subdivided to the *ab interno* and *ab externo* approaches, in which an incision is made within the retina or within the sclera, choriocapillaris, or RPE to insert the device, respectively). There is also the optic nerve approach, in which electrodes are placed around the optic nerve in an attempt to coarsely stimulate the afferent ganglion cell axons [11]. Finally, there are also the cortical approaches, whether they be to the visual cortex [12] or to the lateral geniculate nucleus (LGN) of the thalamus [13, 14], the first stop for information from the retina as it enters the cortex. A complete discussion of the advantages and disadvantages of each of the different approaches is beyond the scope of this text, but can be found in several good review articles on visual and retinal prostheses.

The harbinger of an epiretinal prosthesis was the successful demonstration of a prototype 16-electrode device, fabricated by Second Sight Medical Products, Inc. (Sylmar, CA, USA) in six patients [15]. While clearly not enabling such activities of daily living as newspaper reading and facial recognition, previously completely blind subjects can, for instance, differentiate between a plate, a cup, and a knife, in a high-contrast environment free from background distracters, an undeniably incredible feat of engineering and medicine. Furthermore, subjects have been shown to be able to discriminate direction of movement of parallel white bars on a black background, and can locate white squares within a quadrant of otherwise black space [16]. This implant demonstrated the technology as well as the remarkable ability for the human brain to compensate for low-resolution input. Although this had previously been demonstrated by cochlear prostheses for patients with severe hearing impediments [17], it was unclear whether this plasticity would translate well to visual prostheses. In fact, patients have demonstrated their ability to discriminate large letters simply by *instinctively* scanning the camera mounted on their head back and forth over the image displayed in front of them, a sort of innate edge-detection mechanism, dramatically increasing the capability of the 16-electrode device on their retina. Few scientists disagree, however, that increasing the number of electrodes on the implanted array will dramatically add to the capabilities of the prosthesis as a whole in enabling the patient to better carry out activities of daily living. The prototype device

is hand assembled, a fact that limits the resolution possibilities of the device. Indeed, were it still necessary to interconnect integrated circuits by hand, computers would be far less useful to us as they are today. The need exists, then, to bring microelectronics and microfabrication technology to bear on the problem of retinal prosthetic devices. The race is on to build high-density multielectrode arrays in such a way and with such materials that the method is scalable to the needs of long term, high-density retinal stimulation. Recently, a sixty electrode version of the epiretinal prosthesis has been tested and has gained the CE Mark in Europe for sale for the treatment of retinitis pigmentosa. The FDA is now reviewing the results of these same studies for potential approval in the United States as a therapy for outer retinal blindness.

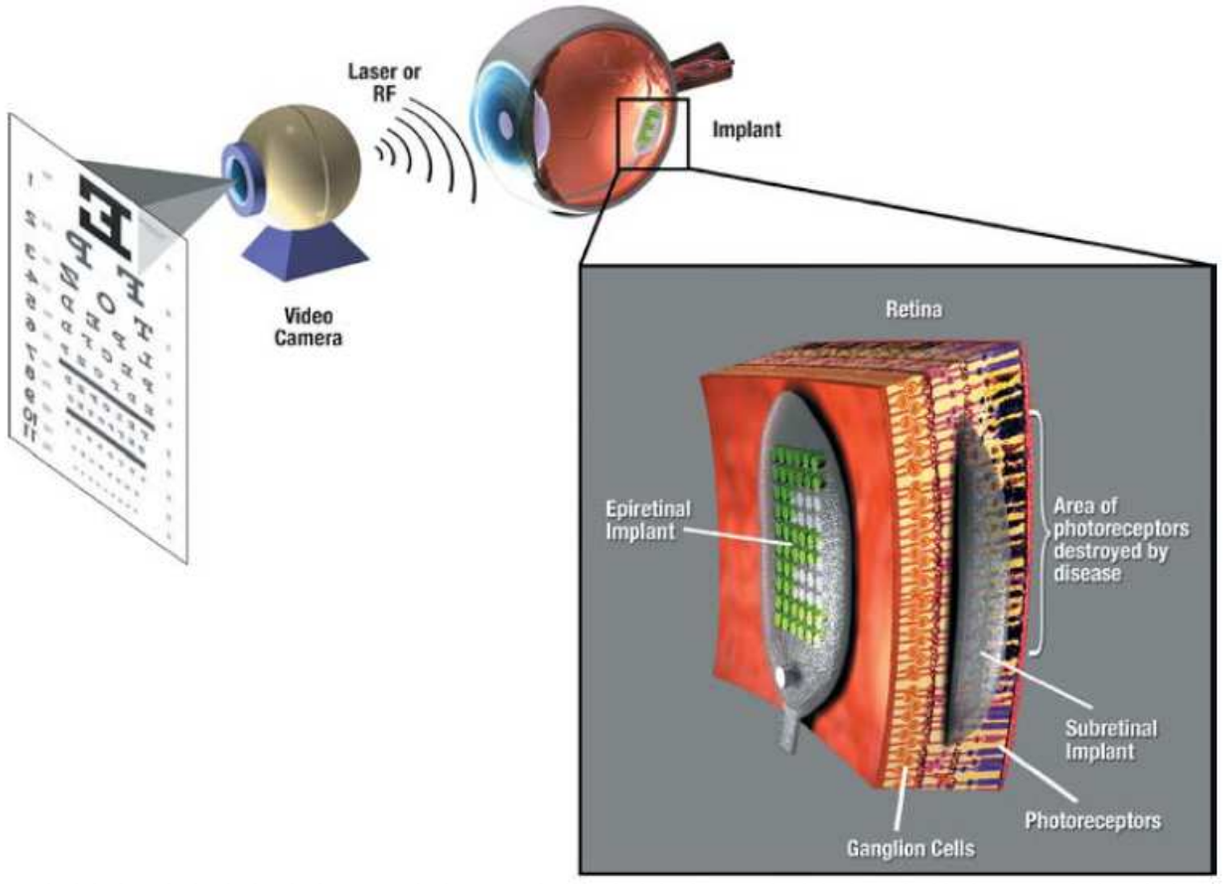

Figure 1. System overview and relative locations of epiretinal and subretinal implants [18].

3. Spinal cord injury

Spinal cord injury (SCI) can occur through a variety of mechanisms. The primary modalities fall into two major categories: trauma (e.g., automobile/motorcycle accident, sports injury such as from diving or horse riding, violence, fall), or disease (e.g., spina bifida or tumor). Spinal cord injuries can affect motor function, sensation, and autonomic functions (e.g., bladder

control, breathing). Approximately 50% of SCIs in the United States are classified as complete [19]. This means that the spinal cord has lost the ability to transmit information across a segment within it, cutting off all functional communication from the brain to the nerves below the injury site and resulting in no sensation or voluntary control of motor function below the injury site due to lost input from the brain. This usually results in para- or quadriplegia, depending on the site of injury. Although in most cases the cord is not completely transected or even cut, it is significantly damaged by interruption of blood flow supplying one of its segments or through spinal contusion. Even though the vertebral column protects the cord, when trauma is sufficient to compromise this protective cage, the broken vertebrae can impinge on the cord and crush or destroy the axons within it very quickly, with continued loss of axons over time [20]. Some estimates pin the prevalence of spinal cord injury in the United States at approximately 250,000 [21], with an incidence of approximately 10,000 to 12,000 per year [22], while others state the prevalence is significantly higher, at around 450,000 [19]. Approximately 55% of spinal cord injuries occur in young victims between 16 and 30 years of age, making it a disease to bear usually for the rest of their lifetime, and more than 80% of victims are males [22]. In some cases of incomplete injury, function can be recovered over time [23]. However, in most cases, some level of impairment is permanent.

The complexity of the spinal cord is undeniable. In fact, despite the popular misconception that the spinal cord serves only as a communication conduit between the brain to the muscles and organs and from the skin back to the brain, it is much more accurate to view the spinal cord as an extension of the brain. While the spinal cord below a complete injury does indeed lose input from the motor cortex, and its ability to send sensations of touch to the brain is completely compromised, the spinal cord is not rendered useless. Even an intact cord does a lot of the primary processing and reflex control without any input to or from the brain.

In patients with spinal cord injury, there are several approaches to rehabilitation. The foot-drop stimulator, wherein stimulation of the peroneal nerve affects localized contraction of ankle dorsiflexors to counteract the problem of foot drag, has been widely studied [24] with mixed results [25-27]. Other functional movements requiring much more coordinated musculature responses are far more difficult with implantable peripheral nerve or muscle stimulators because of the need to control timing as well as pulse amplitudes of likely a large number of electrodes in rapid succession. Skin surface electrodes such as those in the ParaStep system [28, 29] suffer from these problems as well as the problem that many muscle groups are difficult to target from this more remote location. In addition, because in complete SCIs the voluntary input from the motor cortex to initiate such movements is lost, an accessory mechanism for determining the desired motion is warranted. This may require recording electrode arrays in the motor cortex as another component of this system, as well as possible electrical stimulatory feedback (in addition to the visual feedback already present). Any such system, then, is likely to be quite complex and difficult to implement in practice.

We propose a system, which eventually will be completely implantable, that is capable of stimulating the dorsum of the spinal cord in such a manner that modulation of the sensory input to the cord, interneruonal activity within, and even motor output from the cord, is possible. Tonic, subthreshold stimulation, applied at precise times and precise locations along

the spinal cord, would likely help sustain or stop locomotor activity with the kind of coordination and rhythmicity already discussed. Perhaps in combination with both locomotor and standing training as well as appropriate pharmacological administration (e.g., quipazine), it is possible that such an array would give those with both complete and incomplete spinal injury the ability to stand and walk once again. In order to provide appropriate proprioceptive input in the case of complete SCI, it would likely be possible to provide an accessory device or muscle stimulator to initiate this type of activity. However, this approach leverages the innate activity and processing power present in the spinal cord to its greatest extent and likely obviates the need for a stimulation control system of great complexity in order to bring about coordinated muscle activity, as is necessary for a peripheral muscle or motor neuron control system. Such electrical stimulation may also, as has been hypothesized in the case of subthreshold retinal stimulation systems as well, have the capability of promoting axon regrowth [30, 31] and facilitating plastic changes in the cord. Such an array would likely need to be conformable to the cord, and would need to be implanted in relatively close apposition to it, either epidurally (from which location the electrical field would need to penetrate several meningeal layers) or subdurally, such that it is closer to the surface of the cord. In the ideal case, the array would be flexible enough to move with the cord during motion and bending such that functional targets are the same in any position. In addition, it should be the case that such an array can also record from the cord so as to recognize returning action potentials from the dorsal root and modulate this input accordingly. This approach, then, requires a high-density array with many electrode sites from which to choose during training and daily activity, as well as the ability to both record from and stimulate the cord, something which current arrays, such as those for pain management, simply can not do because they are too bulky, inflexible, and of too low a density (up to 16 electrodes).

4. Introduction to parylene

Parylene is the trade name for a family of semicrystalline thermoplastic polymers known as the poly(para-xylylenes) (PPX). These were discovered in 1947 by Michael Szwarc in Manchester, England [32]. It was originally deposited in an investigation of aliphatic carbon-hydrogen bonds where the carbon was attached directly to a benzene ring, by heating toluenes and ortho-, meta- and para-xylenes to very high temperatures and looking for degradation products [33]. The very first parylene film deposited, then, was parylene N (with no substitutions on the benzene ring), and was temporarily known as a Szwarcite snakeskin. This deposition process, however, had the disadvantage that gaseous by-products were an inherent part of the method. William Gorham, an employee at Union Carbide, soon thereafter devised an alternate method of parylene deposition that involved the pyrolysis of a dimerized form of the material, di-para-xylylene, or [2.2] paracyclophane. It was largely unknown at the time how to make this dimer in large amounts as it had only been isolated as an impurity in Szwarc's method. However, in 1951 Donald Cram reported a method for making this material in bulk. On February 17, 1965, Union Carbide announced the availability of parylene films and the new vacuum deposition method, known as the Gorham process. There were over 20 types of

http://dx.doi.org/10.5772/55308

parylene actually developed, but only three were considered commercially viable: these were parylene N (no chlorines on the benzene ring), parylene C (one chlorine on the benzene ring), and parylene D (with two chlorines on the benzene ring) (Figure 2). However, a new fluorinated version of parylene, parylene HT, has recently become commercially available, and can be deposited in a new parylene deposition system.

In the Gorham vapor-deposition process [34] (depicted in Figure 3), which takes place at vacuum (~25-35 mT, to increase mean free path to the substrate), a charge of parylene dimer is placed in a vaporizer furnace. The dimer evaporates at approximately 130 to 150 °C, and then passes through a very high temperature pyrolysis (~650 to 750 °C) furnace, where the molecule is split into monomers. The monomers enter a chamber that is held at room temperature, and polymerize on all exposed surfaces in the chamber conformally and without pinholes. Residual monomer is collected on a cold trap. Different variants of parylene require varying process conditions, but the method remains essentially the same.

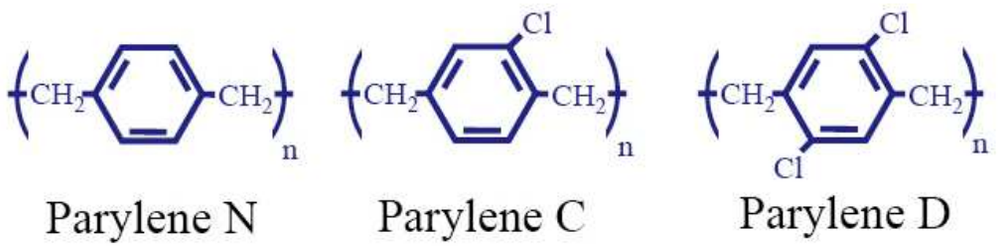

Figure 2. The three originally commercialized parylene variants.

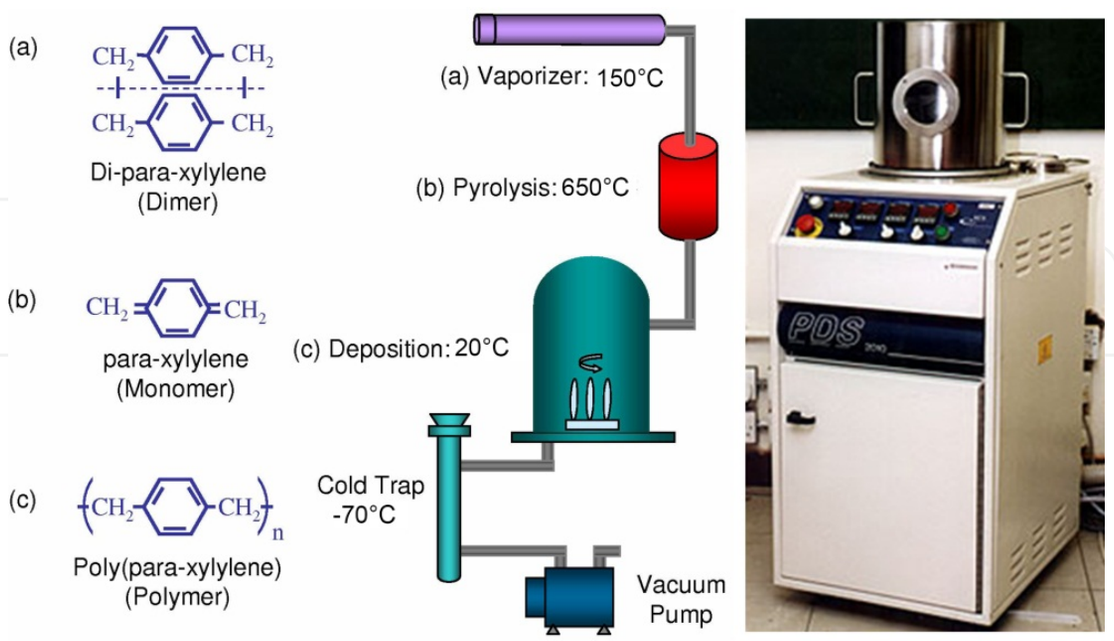

Figure 3. center) Gorham process for parylene deposition. (left) Chemical structures at corresponding points. (right) PDS 2010 Labcoater System.

The existing variants of parylene have varying properties as well as uses. Parylene N is primarily used as a dielectric and when lubricity and crevice penetration is important. Parylene C is an ISO 10993, United States Pharmacopeia (USP) Class VI material (the highest biocompatibility rating for plastics in the United States) and has excellent water barrier properties. In addition, it has a very large elongation to break. Parylene D has now been largely replaced by parylene HT [35], but is used when mechanical strength is of primary concern. Parylene HT has extremely low coefficients of static and kinetic friction, excellent thermal stability and good water barrier properties, high ultraviolet stability, and is also ISO 10993 biocompatible [35-37]. Finally, very recently, Kishimoto Sangyo Co., Ltd. in Japan has devised additional parylenes in which amino groups have been added to the benzene rings. The amino group may add even more improved biostability, but could also generate bioactivity that may or may not be beneficial to device functionality. We have preliminarily tested these amino parylenes have found them to be compatible with standard parylene processing technology, such as oxygen plasma reactive-ion etching (RIE), in our cleanroom, but they will not be explored further in this text.

The advantages of using parylene, and, more specifically, parylene C, as the structural material for neuroprostheses, when compared with technologies based on the use of other materials such as PDMS, polyimide [38] and silicon [39], include parylene's pinhole-free conformality due to its unique room-temperature chemical vapor deposition process, its low water permeability, its chronic implantability and its high flexibility and mechanical strength (Young's modulus ~4 GPa). The Young's moduli of two other commonly used materials for neuroprostheses, PDMS and polyimide 2611, are graphed alongside that of parylene C in Figure 4. PDMS arrays have been handled by surgeons in our vivarium, and these are often as reported as too floppy and difficult to handle due in part to the low Young's modulus, hence requiring very large thicknesses to handle appropriately. In addition, polyimide 2611 (often chosen because its water permeability is lower than that of other polyimides) has a Young's modulus larger than that of parylene C. It has been suggested that polyimide arrays often are too rigid and can damage the retina. In addition, they tear quite easily. Parylene C handles very well under surgical manipulation, and, as we will show, behaves very well when implanted. In addition, the thickness of parylene films is determined by the mass of dimer placed in the vaporizer. As such, thicknesses can be very thin or very thick, and thicknesses are very repeatable and well controlled, more so than spin-on coatings, especially when deposited over step junctions. Parylene thickness can be controlled so as to match the rigidity to the application of interest, more easily than most other materials. Since parylene is deposited at room temperature (we have verified this using Temp-Plate irreversible temperature recorders traceable to NIST (Wahl Instruments, Inc., Asheville, NC, USA)), the coating process is post-IC compatible. Parylene C is also optically transparent, enabling the anatomy to be seen through the cable and the array during ophthalmic surgery, post-implantation examination, and follow-up. While many groups use parylene C as a coating on their arrays for many of these reasons, we have chosen to use it as the main substrate for our devices [40, 41], a paradigm that leverages these advantages to the greatest extent.

http://dx.doi.org/10.5772/55308

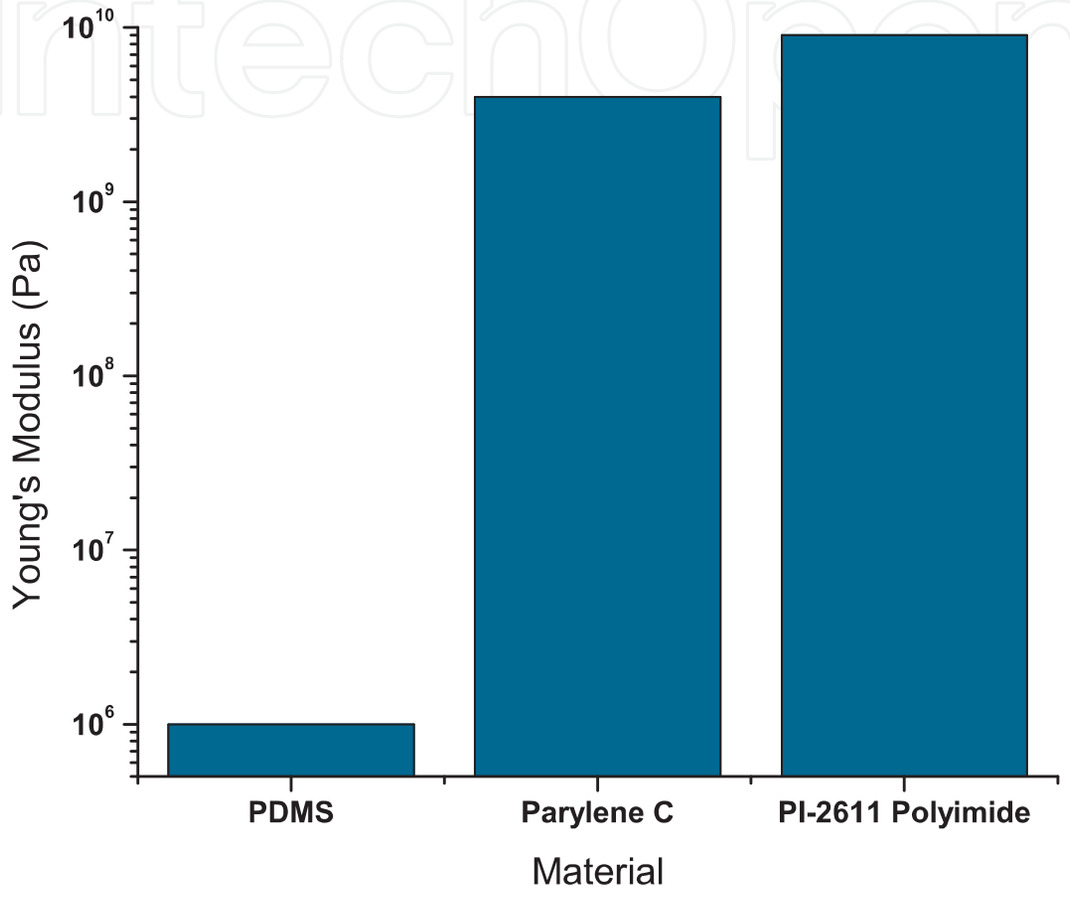

Figure 4. Comparison of Young's moduli of various materials. Ordinate is logarithmic.

Although parylene is known to be biocompatible in many sites of implantation, in order to initially assess the intraocular biocompatibility of the material in the unique immune environment of the eye, an approximately 2 cm × 0.5 cm piece of unmodified 20 μm thick parylene C was implanted in the vitreous cavity of the right eyes of two rabbits for six months. The retinas of the right eyes of both rabbits were compared post-mortem with those of their left eyes that served as controls. Histological evaluation revealed no discernable difference between right and left eyes, indicating that there was no detectable adverse retinitis, choroiditis, endophthalmitis, or scleritis seen as a result of parylene implantation in the vitreous cavity [40]. These results supported the tenet that parylene C is a biocompatible bulk material

for an intraocular retinal prosthesis and other ocular implants, and paved the way for the design and fabrication of a flexible electrode arrays and a packaging system using parylene C as the primary substrate. Given these biocompatibility results, we have also been investigating parylene in several other ocular implants, with excellent results to date [42-44]. Similar experiments were performed with parylene C implanted on the spinal cord of mice. The arrays were well tolerated, with no obvious immune reaction or gliosis.

5. Single-metal-layer flexible MEAs

5.1. Fabrication

Single-metal-layer parylene C-based electrode arrays are fabricated as shown in Figure 5. A photoresist sacrificial layer is optionally spun on a standard silicon wafer. Approximately 8 μm of parylene C is then vapor deposited in a PDS2010 system (Specialty Coating Systems, Indianapolis, IN, USA) on the entire wafer. An LOR3B photoresist layer (Microchem Corp., Newton, MA, USA) and an AZ1518 layer (AZ Electronic Materials, Branchburg, NJ, USA) are spun on top of the parylene, exposed in a 10X reduction GCA Mann 4800 DSW wafer stepper (General Signal Corporation, Stamford, CT, USA) or a Kasper 2001 contact aligner (Kasper Instruments, Inc., Sunnyvale, CA, USA) depending on the required resolution of the electrode array, and developed to achieve a liftoff pattern comprising contacts, conductive traces, and electrodes. After hard bake, approximately 2000 Å to 5000 Å of platinum, with or without a 200 Å titanium layer, is then e-beam evaporated (SE600 RAP, CHA Industries, Fremont, CA, USA) on the wafer. The subsequent photoresist strip generates the desired single-layer metallization pattern. An approximately 7 μm thick coating of parylene C is then deposited, followed by a spin coating of photoresist. This photoresist etch mask is exposed over the areas of the electrodes and contact pads and to pattern the overall array geometry, and the entire wafer is then subjected to an RIE in oxygen plasma, removing the parylene insulation over the electrodes and the parylene surrounding the array. The photoresist mask is then removed with solvent. Finally, if a sacrificial photoresist layer was used, the array is released from the substrate in an acetone bath. If no sacrificial layer was used, it is peeled from the silicon in a water bath. Ultimately, for most cases, the sacrificial photoresist layer is unnecessary, and can often complicate array fabrication due to cracking while under process. The arrays can be easily released from a natively oxidized silicon surface by placing them in a deionized water bath and peeling them from their edge. The water will then release the rest of the structure due to the hydrophobicity of the underlying parylene surface.

A single-layer square-grid electrode array, consisting of 256 Ti/Pt thin-film electrodes 125 μm in diameter in a 16 × 16 grid with connecting lines of 12 μm pitch fabricated in the manner of Figure 5 is shown in Figure 6. An SEM highlighting the typical electrode morphology in such structures is shown in Figure 7. As can be seen, the parylene covering the electrode has been completely removed, whereas the incoming trace remains conformally coated with the material.

http://dx.doi.org/10.5772/55308

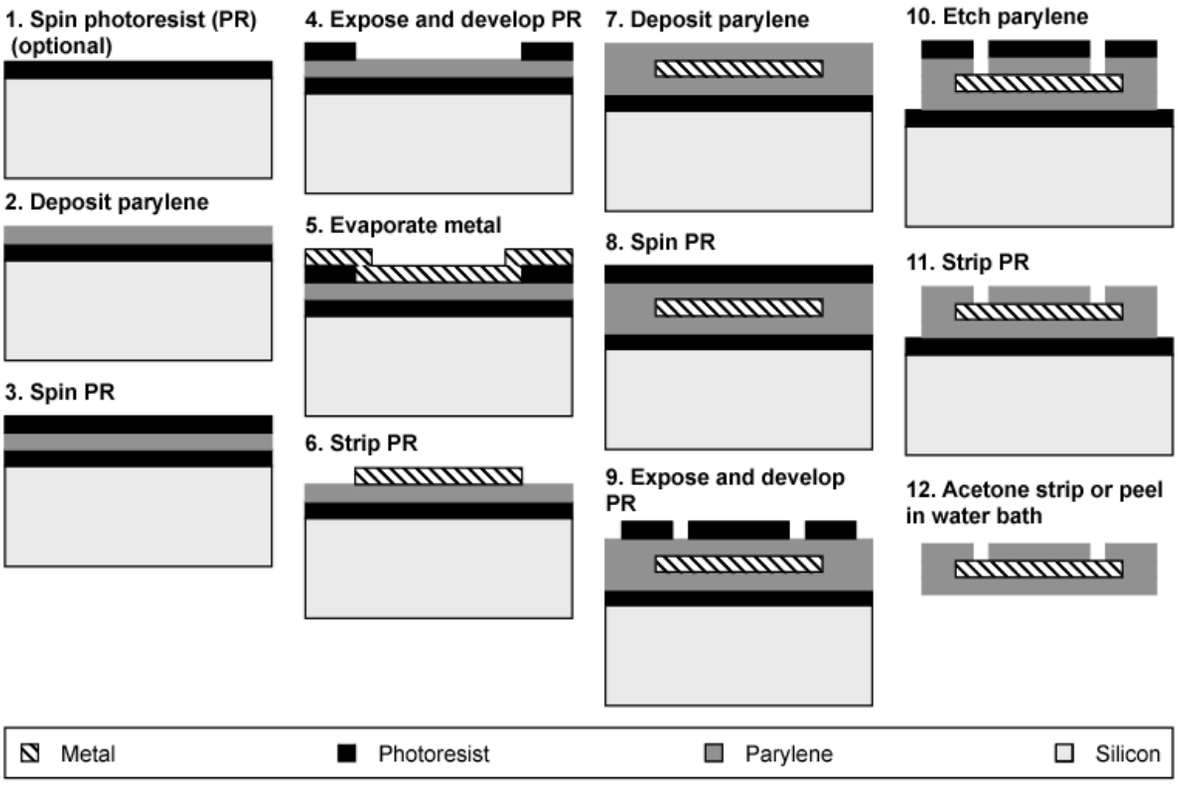

Figure 5. Fabrication process for parylene-based single-metal-layer flexible MEAs.

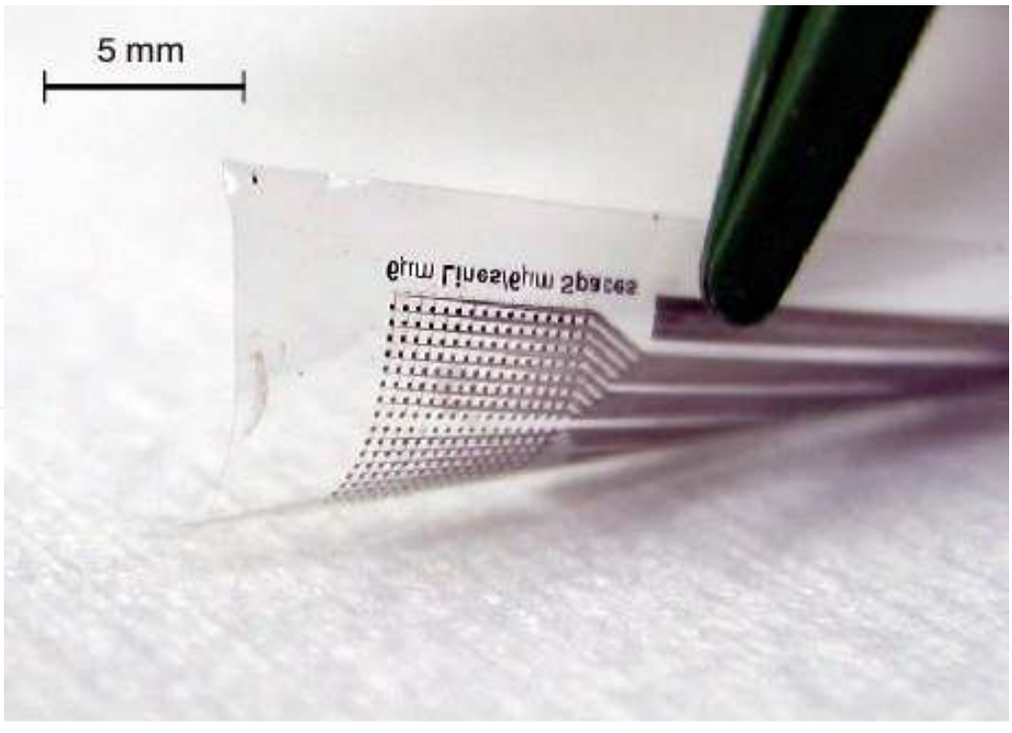

Figure 6. Photograph of Ti/Pt electrode array of 256 electrodes and lines of 12 µm pitch.

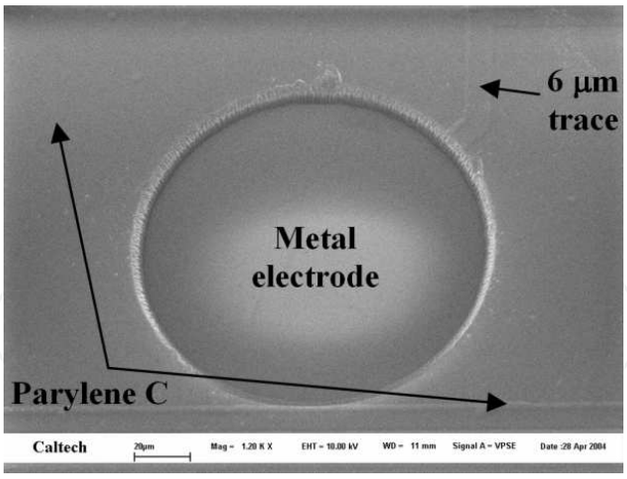

Figure 7. SEM of electrode morphology showing parylene C insulation surrounding exposed metal electrode.

5.2. *In vitro* retinal recording and stimulation

Parylene C-based arrays of thin-film platinum electrodes, comprising four 200 µm diameter stimulating electrodes and 56 recording electrodes of 10 µm diameter were fabricated according to the single-metal-layer process on a glass substrate. These were placed in a bicarbonate perfusate under a microscope and connected to a stimulus generator and preamplification board (Multi Channel Systems MCS GmbH, Reutlingen, Germany) [45]. As shown in Figure 8, a retina isolated from larval tiger salamander (*Ambystoma tigrinum*) was placed RGC side down on the array (to simulate epiretinal stimulation), and a remote platinum ground electrode was introduced to the bath.

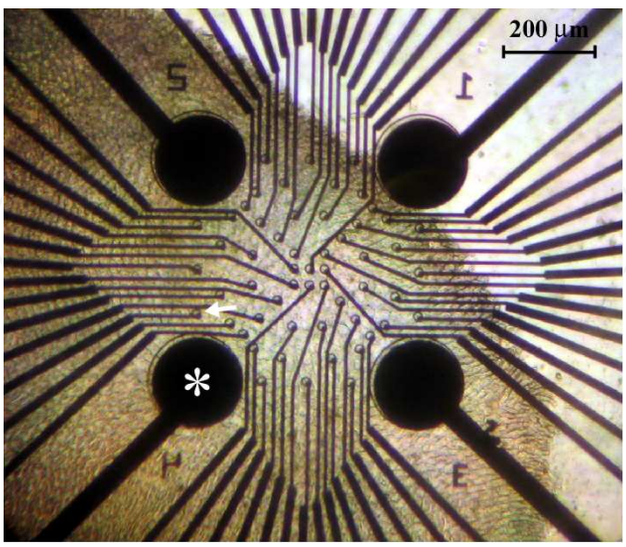

Figure 8. Isolated larval tiger salamander retina (darker region at left) overlying parylene-based platinum electrode array. Arrow indicates 10 µm diameter electrode used for recording trace in Figure 9. Asterisk identifies 200 µm diameter stimulating electrode used to generate action potentials seen in Figure 9.

http://dx.doi.org/10.5772/55308

With the lights off, a 20 μA, 400 μs/phase, cathodic-first biphasic electrical pulse was applied between the stimulating electrode indicated with an asterisk in Figure 8 and the ground electrode. The voltage trace from the recording electrode is shown in Figure 9. This stimulation was consistently repeatable over a 50 pulse train with a 400 ms inter-pulse interval, and other stimulating electrodes were also capable of "epiretinally" stimulating other cells in the retinal slice. As is clear from these results, the parylene-based platinum electrode was able to stimulate the tissue and elicit a response similar to the response generated from a light pulse in this intact retina. Given these results and the knowledge garnered from clinical trials with prototype arrays fabricated of other materials, it is not unreasonable to presume that our arrays will most likely be able to stimulate retinal tissue in other species, including human.

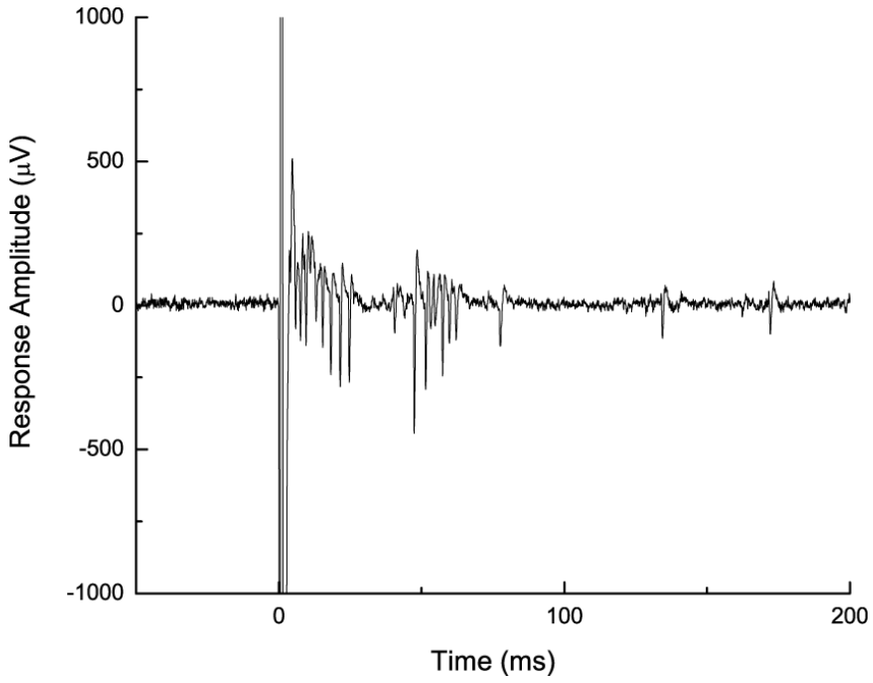

Figure 9. Typical recording of response of cells overlying recording electrode to a 20 μA, 400 μs/phase, cathodic-first biphasic electrical pulse from "epiretinal" stimulating parylene-based platinum electrode denoted with an asterisk in Figure 8.

6. Spinal cord prosthesis

6.1. System overview

The ideal spinal cord stimulation system, just like the retinal system, would have a power source, circuitry for driving the appropriate electrodes, as well as a cable and electrode array, this time implanted epidurally or subdurally on the spinal cord. We believe that a penetrating electrode array would be problematic for implantation and would likely lose efficacy and fail ultimately due to a gliosis over time, as has been shown in many other studies [27]. The power source could be an RF coil, or could, due to the much larger space available in the abdomen

and back as compared with the eye, be a rechargeable battery capable of charging through the inductive link. The RF coil, in addition, would enable reprogramming of the implanted electronics for alternative stimulation protocols at the physician's discretion. The electrode array should be conformable to the spinal cord so that it can tonically stimulate at low currents and with high precision. While a completely implantable system is the ultimate goal, an interim goal is to stimulate the spinal cord chronically from an array connected to a head plug, while simultaneously being able to record electromyograms (EMGs). In order to achieve this, we have studied the efficacy of the multielectrode array portion of this system and have begun to develop a connector technology capable of connecting 36 electrodes in with a small enough form factor to be chronically mounted on a mouse skull.

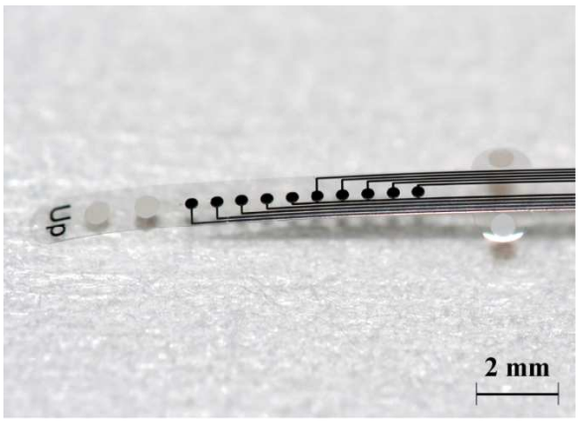

Figure 10. Parylene MEA for murine spinal cord stimulation and recording.

6.2. Fabrication

Spinal cord arrays, consisting of five or ten electrodes of 250 μm diameter were designed and fabricated (Figure 10). Interelectrode spacing was controlled so that each array of electrodes covered four to five segments of the murine lumbosacral spinal cord upon implantation. Suture holes were also designed into the body of the array to ensure placement and attachment of the array on the cord, as well as to facilitate implantation (suture can be attached to the end of the array and can be threaded along the cord first to help direct the array along it).

The single-metal layer fabrication process was performed using a contact aligner process for fast throughput. The fabricated arrays were annealed to increase the adhesion of parylene to parylene. At the same time, they were clamped between two pieces of Teflon or glass slides coated with aluminum foil to ensure they would be flat during implantation. The arrays were connected via Clincher connectors (FCI, Versailles Cedex, France) to the stimulation and recording electronics.

6.3. Implantation and testing

Just prior to implantation, the arrays were rinsed in isopropyl alcohol. Under isoflurane anesthesia, the spinal cord electrode arrays were implanted epidurally on spinal cord seg-

http://dx.doi.org/10.5772/55308

ments L2-S1 in nontransected mice. The electrodes were oriented linearly along the rostrocaudal extent of the cord. Recording capability was assessed by using the electrode array to record spinal cord potentials evoked by tibial nerve stimulation. Following stimulation of the tibial nerve, somatosensory evoked potentials were recorded from the cord dorsum at three lumbosacral levels (P1-P3, rostral to caudal). The recorded waveform consisted of three response peaks, two of which are clearly depicted in Figure 11 (N1 and N3). These findings closely mirror results reported previously in a study using conventional spinal cord recording electrodes [46] demonstrating that the recording capability of the array electrodes matches that of conventional electrodes. By measuring the difference in the response latencies obtained at each electrode position (corresponding to different levels of the spinal cord), and by utilizing the known, fixed interelectrode spacing, accurate measurements of the conduction velocities were obtained. The properties of these responses can potentially be used to diagnose the progressive recovery of the spinal cord as a result of treatments provided after a spinal cord injury.

To test the capability of the electrode array to act as a multichannel stimulating device for generating hindlimb movements, constant-current monophasic stimulus pulses (amplitude: 50-850 μA, frequency: 0.3-10 Hz, pulse duration: 0.5 ms) were applied to the spinal cord between each of the array electrodes and a ground electrode located near the shoulder, while muscle activity was monitored using electromyogram (EMG) recordings of the tibialis anterior and medial gastrocnemius muscles. Stimulation generated a typical three-component EMG action potential consisting of an early (direct motor), a middle (monosynaptic), and a late (polysynaptic) response, classified by post-stimulus latency (Figure 12). These data clearly indicate that the parylene arrays were able to stimulate the spinal cord in such a way that the musculature was activated.

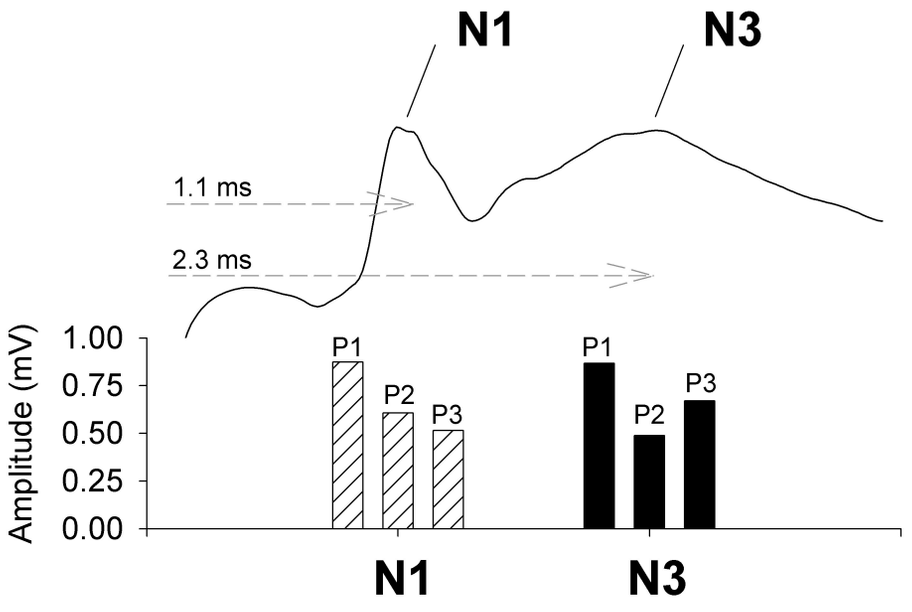

Figure 11. Peak amplitudes of somatosensory evoked potentials (N1 and N3) recorded from three levels of the rostrocaudal spinal cord (P1-P3). Example waveform at top shows approximate response times.

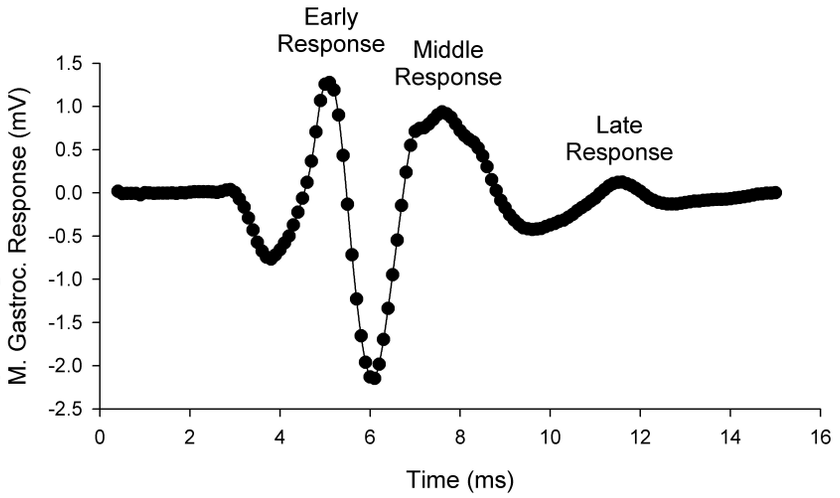

Figure 12. Typical medial gastrocnemius (ankle plantarflexor) EMG recording showing early, middle, and late responses after stimulation of spinal cord with parylene MEA.

Because of the known spacing of the electrodes on the array (as compared with traditional fine-wire electrodes which do not have known interelectrode spacing), we were able, in addition, to determine whether electrode position had a significant impact on muscle recruitment. The appearance and magnitude of each of the EMG responses was indeed correlated with the choice of electrode position (Figure 13). This serves as evidence that position of stimulation is very important. With a one-dimensional array, it is difficult to assess whether a bilateral stimulation paradigm would also result in lateralization of response, but we strongly suspect that this would be the case.

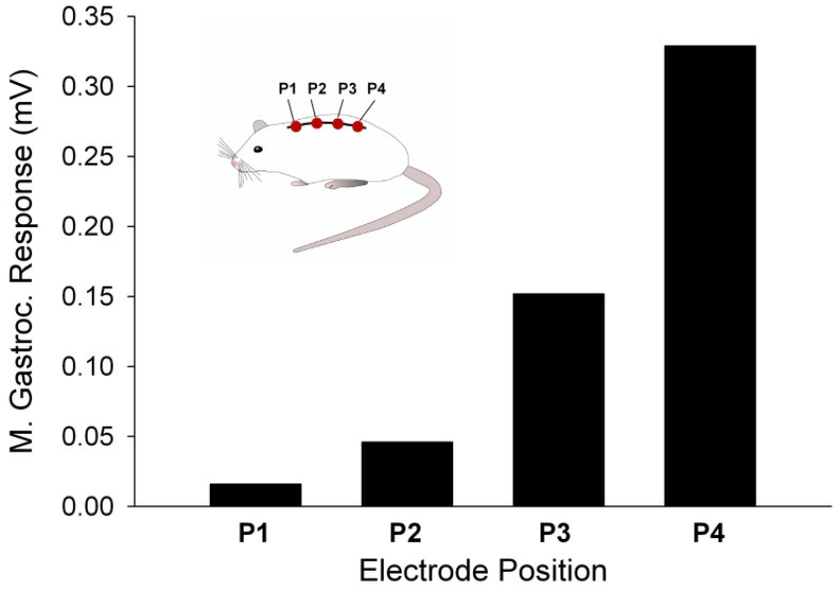

Figure 13. Medial gastrocnemius EMG showing varying levels of activation due to stimulation at different rostrocaudally located electrode sites.

7. Dual-metal-layer flexible MEAs

7.1. Motivation

An inherent problem with single-metal-layer arrays is that electrodes and traces are necessarily fabricated alongside each other. For high-lead-count devices, this limits the size of electrodes and tends to crowd electrodes and traces into artificial groups. To allay these problems, a dual-metal-layer approach was devised that enables traces to pass underneath overlying electrodes.

7.2. Fabrication

Dual-metal-layer electrode arrays are fabricated as shown in Figure 14. Approximately 8 μm of parylene C is first deposited on a silicon wafer with the optional photoresist sacrificial layer, forming the underside of the electrode array. A platinum or titanium-platinum metal liftoff process is used to define traces with 16 μm pitch and 2000 Å to 3000 Å thickness. A second parylene deposition (~1 μm) forms the insulation between the two metal layers. At this point, 6 μm by 6 μm vias are patterned in the insulation layer over the ends of the traces using an O_2 plasma RIE. A second step-coverage optimized liftoff process is used to define a second metal layer comprising electrodes and traces, while at the same time achieving electrical continuity between the underlying traces and the overlying electrodes. A final parylene coating approximately 7 μm thick forms the top insulation. The electrodes are exposed and the overall geometry of the implant is defined in a final set of O_2 reactive-ion etches using a thick photoresist etch mask. Finally, the arrays are peeled from the wafer in a water bath or released through removal of the sacrificial photoresist in acetone. The process depends on optimal step coverage of the parylene sidewall during evaporation, which is aided, in part, by the slightly isotropic nature of the O_2 plasma etch of parylene [47] as well as by the special design of the rotating wafer domes inside the e-beam evaporator, for which the angle of attack of the metal evaporant is adjusted for best coverage. This requirement conflicts marginally with those for successful metal liftoff, however, in this case, the liftoff technique is robust even under these step-coverage optimized conditions due to the choice of an LOR/positive photoresist compound layer.

7.3. Implantation and testing

Chronically implantable retinal electrode arrays comprising 1024 75 μm diameter electrodes arranged in a complex biomimetic pattern that closely mimics the density of RGC in the human retina [48] were designed (the electrode density varied radially in a ratio matched to that of the RGCs), as shown at the left in Figure 15. These arrays (shown at right in Figure 15) were fabricated according to the dual-layer process, with 60 of the electrodes connected via two traces each to facilitate electrical conductivity verification. The strength of metal adhesion was verified using a Scotch tape test, which demonstrated that direct platinum evaporation is feasible without the need for a titanium adhesion layer. Electrical testing demonstrated a typical line impedance of a contact-electrode-contact circuit to be approximately 5 kΩ, which included two 8 μm wide traces of 20 mm length, as well as two via step junctions connecting

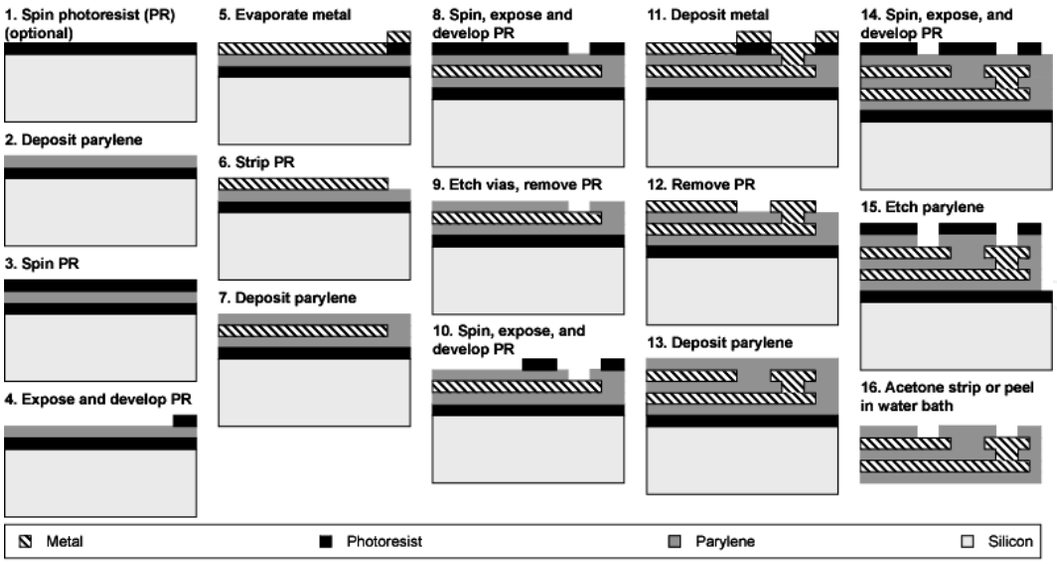

Figure 14. Fabrication process for parylene-based dual-metal-layer flexible MEAs.

underlying traces to the overlying electrode. Two types of via and electrode configurations were tested. Some electrodes (electrode SEM given in Figure 16 (left)) had vias connecting to the underlying trace near the center of the electrode, hence enabling charge spreading from the center of the electrode. One possible drawback to this configuration is that the contact from trace to electrode over the sidewall is a potentially vulnerable point of the circuit during processing (e.g., subsequent RIE processes) and during pulsing in electrolyte because the metal may be thinner there. The other electrode configuration had vias located adjacent to the electrode (electrode SEM given in Figure 16 (right)), with the possible advantage that it would be protected during RIE and subsequent pulsing by the overlying conformal parylene layer. An SEM showing the morphology of a single central via is given in Figure 17. This clearly depicts the sidewall coverage responsible for the electrical contact between the first and the second metal layers. In both configurations, each via had an impedance of less than 12.5 Ω. The best final configuration has not yet been determined.

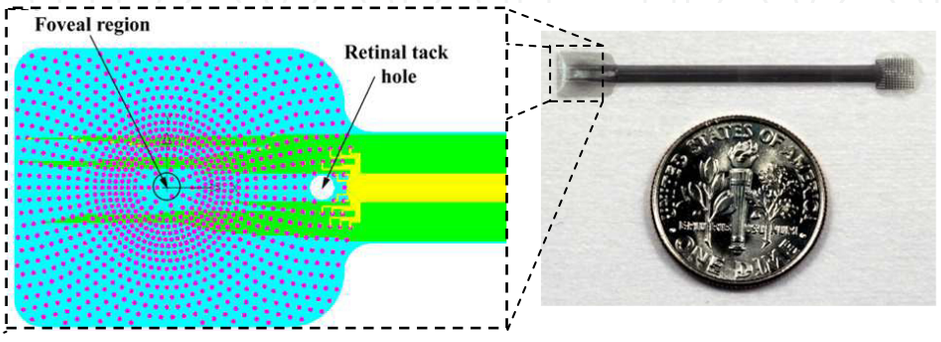

Figure 15. (left) Design of biomimetic dual-metal-layer retinal electrode array showing biomimetic arrangement of electrodes. (right) Fabricated biomimetic chronically implantable arrays with 60 of 1024 75 μm diameter electrodes connected through dual-layer process with U.S. dime for size comparison.

http://dx.doi.org/10.5772/55308

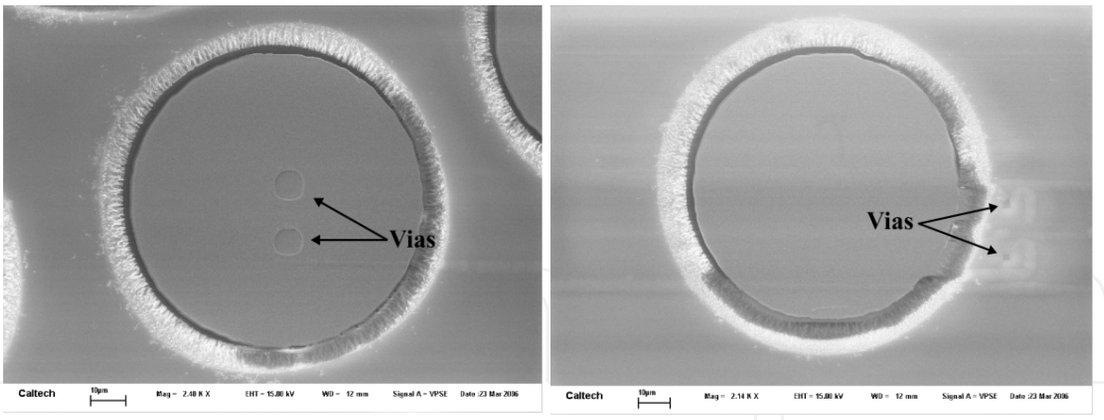

Figure 16. Two possible dual-layer electrode configurations. Electrode with central vias (left), and electrode with abutting vias (right).

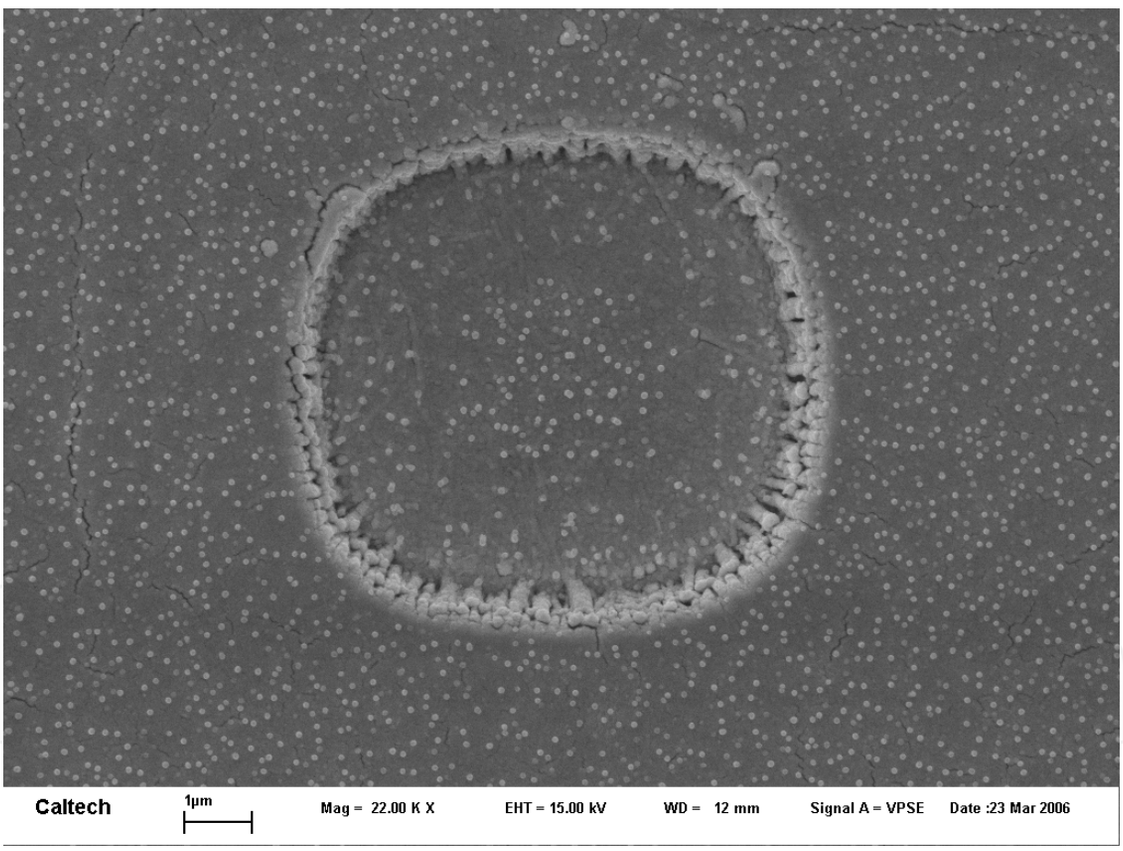

Figure 17. Magnified view of trace to electrode via showing sidewall coverage.

The arrays were successfully molded to the approximate curvature of the canine retina (Figure 18 (top)) using heat-annealing and a custom mold in a vacuum chamber, and sterilized using ethylene oxide gas. Two biomimetic arrays were implanted in the right eye of two canines through a 5 mm pars plana incision after vitrectomy, and were affixed to the retina (Figure

18 (bottom)) using a retinal tack modified by the addition of a PDMS washer (to account for the thin nature of the parylene arrays).

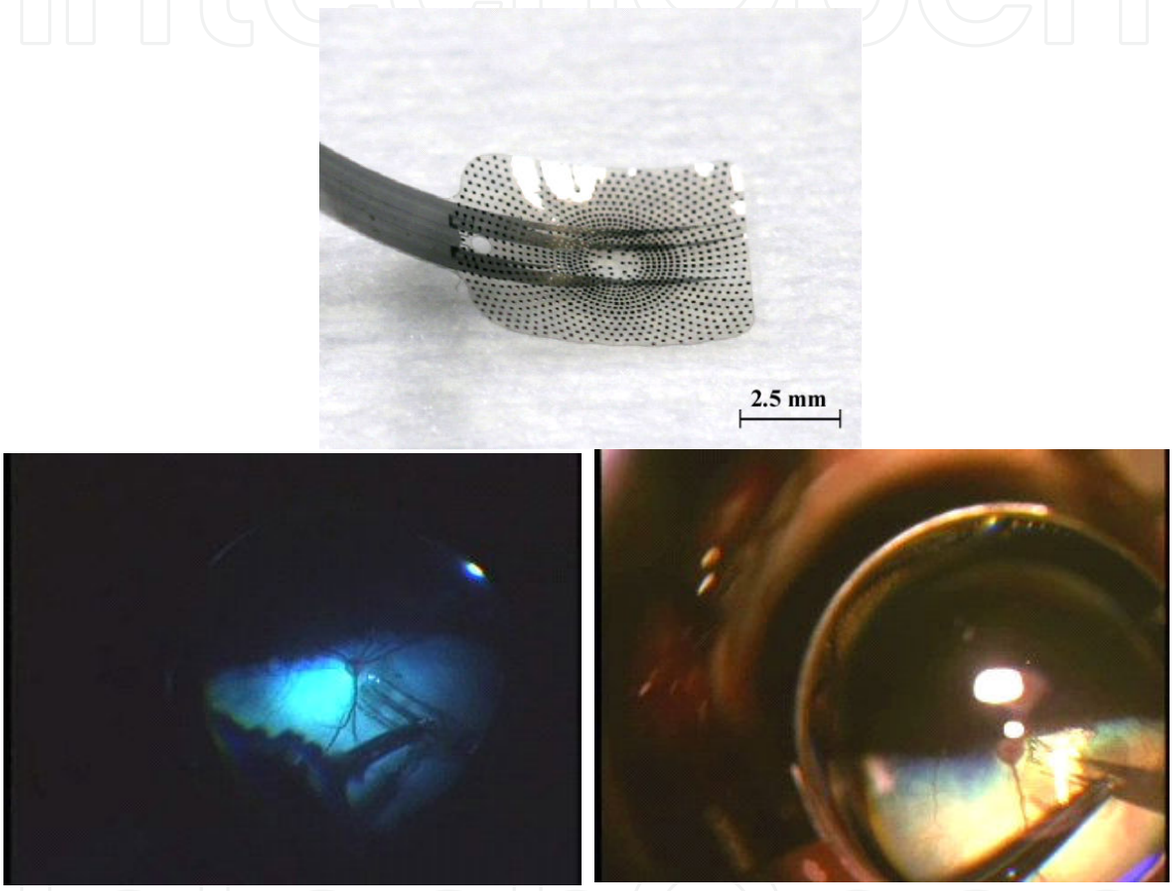

Figure 18. Heat-molded and annealed retinal electrode array with retained spherical curvature (top), and intraoperative photographs of tacking in each canine (bottom).

Follow-up in both animals was conducted for six months using fundus photography, fluorescein angiography (FA), in which blood is fluorescently stained to assess vessel perfusion in the retina, and optical coherence tomography (OCT), an interferometric technique that enables cross-sectional imaging of the retina. Fundus photography and FAs of both animals, examples of which are shown in Figure 19, consistently demonstrated that vessel filling underneath the array was normal. Obstruction and vessel leakage would have been visualized if the array were placing excessive pressure on the retina. In addition, OCT demonstrated that the electrodes were consistently less than 50 μm away from the ganglion cell layer in both animals

http://dx.doi.org/10.5772/55308

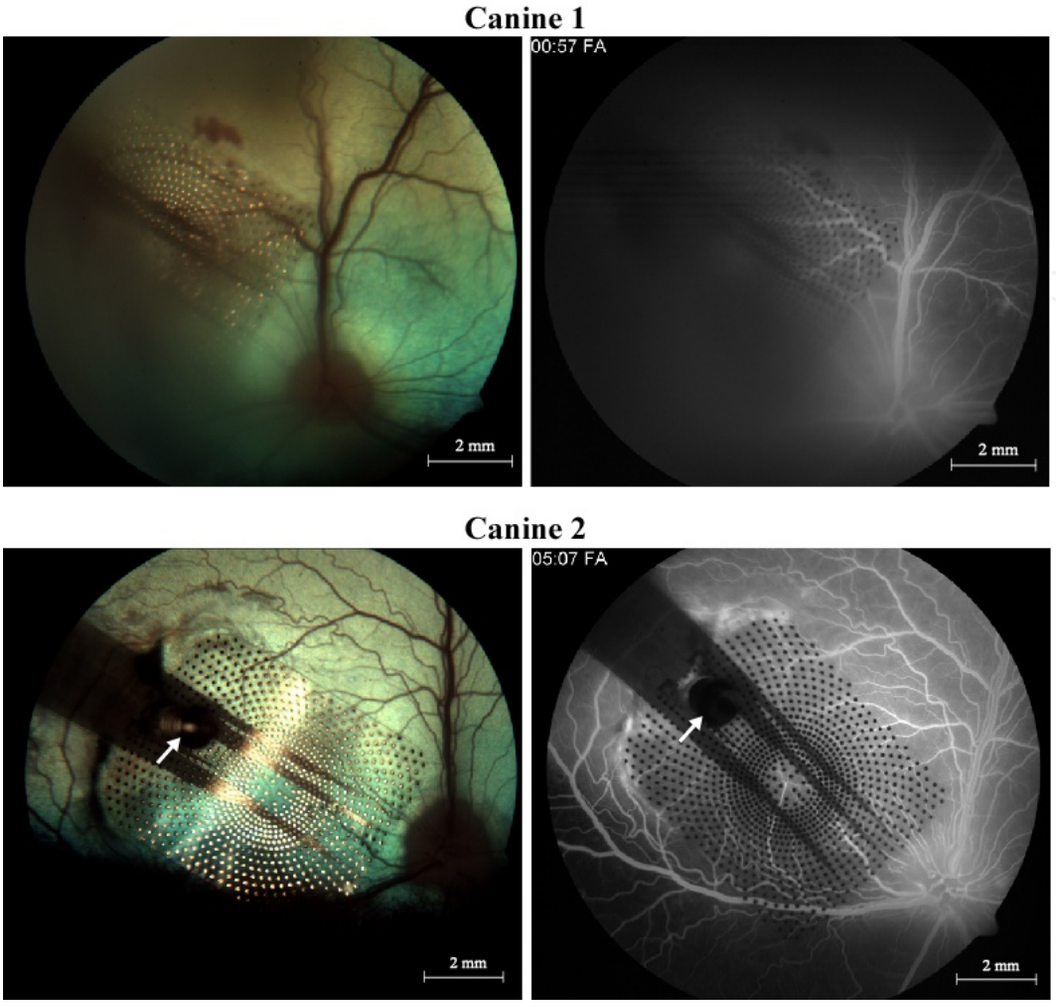

Figure 19. Fundus photographs (left) showing parylene MEAs tacked to the right retina of both animals and FAs (right) showing normal vessel perfusion under the arrays. Arrows point to retinal tacks.

(typical OCTs of both animals are shown in Figure 20), an outcome that theoretically would afford excellent electrical coupling between the electrodes and the electrically excitable cells of the retina. It is important to note that in the OCT of the second canine, the scan was taken along a segment furthest from the tack site, where one might expect the least proximity. Even at this location, this array remained in very close apposition throughout the six-month implantation. Post-enucleation histology has since confirmed the excellent biostability seen during follow-up.

As was briefly mentioned previously, the dual-layer process proffers considerable advantages over the more traditional single-layer approach. Design of single-layer electrode arrays is usually hindered by the need to route traces amongst the electrodes. This tends to cause crowding of traces and electrodes into groups, an organization that may not be optimal for stimulating the tissue of interest. In addition, this has a propensity to constrain the geometric area of the electrodes in the MEAs to smaller sizes, and thus reduces the number of electrodes possible in a given area. The dual-layer process obviates these problems by

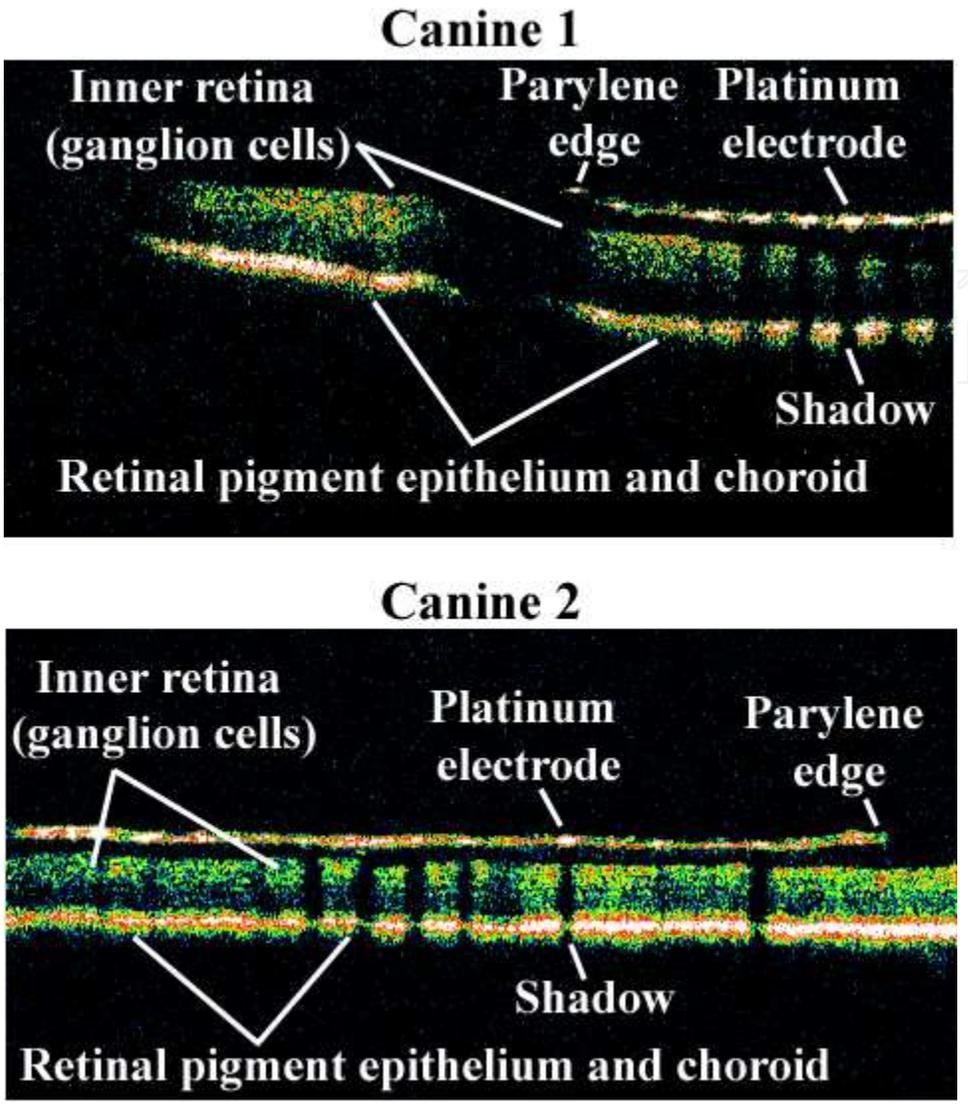

Figure 20. OCTs of both animals showing very close apposition (<50 μm) of the arrays to the RGC layer.

enabling traces to pass under overlying electrodes without making contact to them, having the effect of both relaxing the constraints on electrode size and number and enabling more complex electrode organization (such as the biomimetic one presented in this work). Although the arrays fabricated here had just 60 electrodes of connectivity with 120 traces total, this was without making full use of both layers for wire routing and connection of electrodes. In order to not make traces unnecessarily narrow and of too high impedance, we believe an extension of this process to three or more metal layers will be necessary to achieve 1024 electrodes of total connectivity. Indeed, this fabrication process is easily extendable to create such structures through addition of extra layers of parylene and metal. Given the encouraging biostability results presented here and the ability of these arrays to stimulate retinal tissue, future studies will include chronic stimulation from implanted parylene-based arrays in an animal model.

http://dx.doi.org/10.5772/55308

8. Electroplating

As a possible mechanism for extending the longevity of chronically pulsed electrodes, we have investigated electroplated films of high surface-area platinum. Specially designed thin-film platinum electrode arrays, consisting of sixteen 75 μm and 150 μm diameter electrodes of 3000 μm center-to-center spacing, were fabricated according to the single-layer process. Initial experiments were performed on these arrays to determine material morphologies after plating at different potentials in an aqueous ammonium hexachloroplatinate solution according to Whalen *et al.* [49]. Subsequently, arrays were immersed in the solution in a specialized jig and six were plated at a plating potential of -0.6 V (vs. an Ag/AgCl reference electrode) for 1.5 hours. The others remained unplated. Electrochemical tests were performed to evaluate the efficacy of this plating step in extending electrode longevity under chronic pulsing.

The electrode morphologies of a typical array of 16 electrodes plated at different potentials are shown in Figure 21. Note that the 4 corner electrodes (1, 4, 13, and 16) were not plated. Magnified views of some of the possible morphologies attainable via this mechanism are shown in Figure 22. These micrographs show morphologies that likely correspond to a drastically increased surface area. In order to confirm this cyclic voltammograms (CVs) in O_2-free H_2SO_4 were taken of the electrodes before and after platinization. According to [50], "real" electrode surface area can be adequately estimated by integration of the area over the hydrogen adsorption peak or likewise the area under the hydrogen desorption peak. The two CVs in Figure 23 show that there was a more than 40-fold increase in surface area after platinization when compared with the pre-plated surface area (note the change in scale of the ordinate from nA to μA). Under pulsing, the voltage responses of both plated and unplated electrodes remained stable for approximately 29 days, at which point the unplated electrodes showed signs of failure. Voltage responses for one such electrode on day 26, 29, and 31 are overlaid in Figure 24 (left), which documents the progression of failure. The plated electrodes, on the other hand, remained intact for much longer, most surviving more than 50 days, or 430 million pulses, at which point the testing goal was met and the test was stopped. Overlaid voltage responses for one such electrode, showing the voltage responses at day 26, day 31, and day 50, are shown in Figure 25 (right). The electrochemical impedances at 1 kHz of a typical plated and unplated electrode are shown in Figure 25. A dramatic jump in impedance was observed for the unplated electrode at the time of failure, while the plated electrode demonstrated only minor variability in its lower impedance throughout the 430-million-pulse trial (most variability happened on the days that CVs were taken, as expected). These preliminary data corroborate the evidence that plating of the electrodes is beneficial to longevity, and suggest that high surface-area platinization of electrodes can have a dramatic effect on extending electrode life while lowering electrochemical impedance to charge delivery. Future work will include replication of these tests and chronic pulsing at high temperatures for longer times to further accelerate and assess the possible modes of failure.

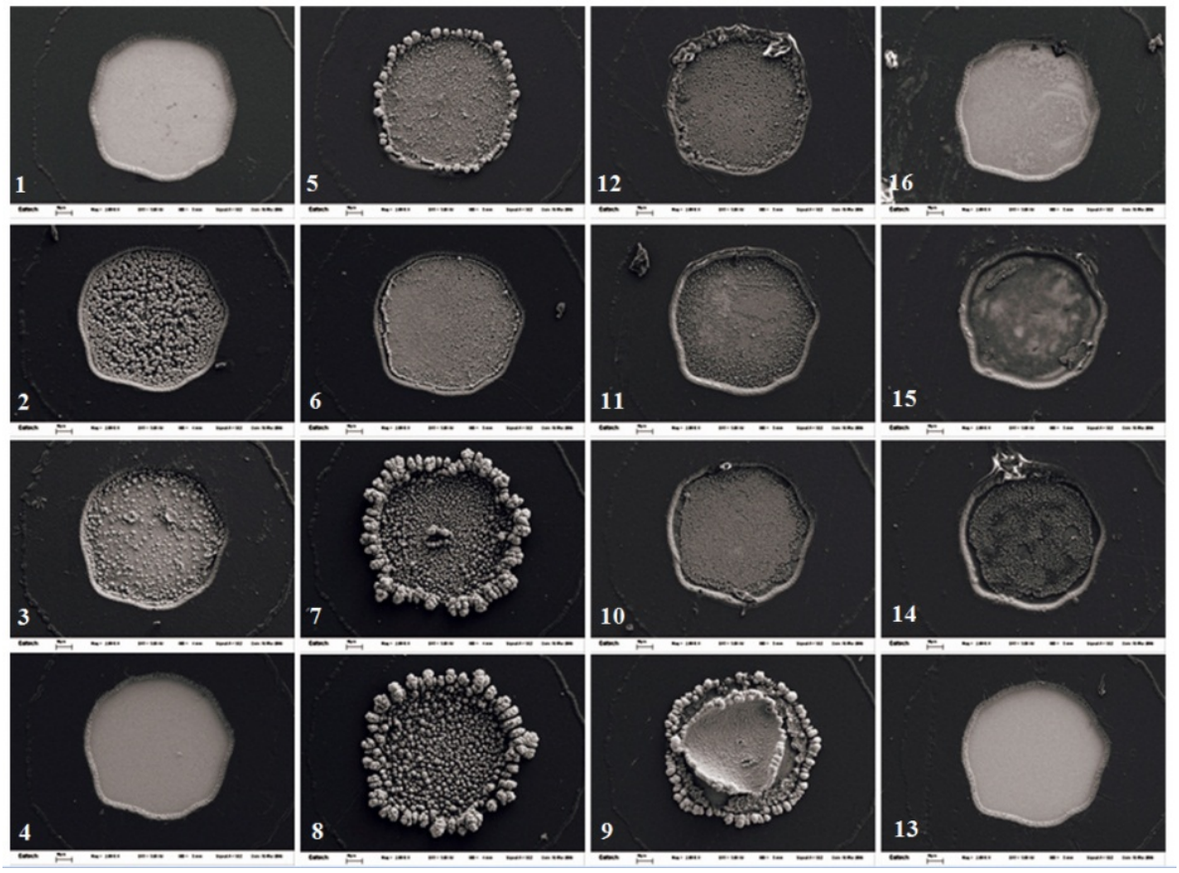

Figure 21. SEM of each of the electrodes on a typical 16-electrode array after platinization.

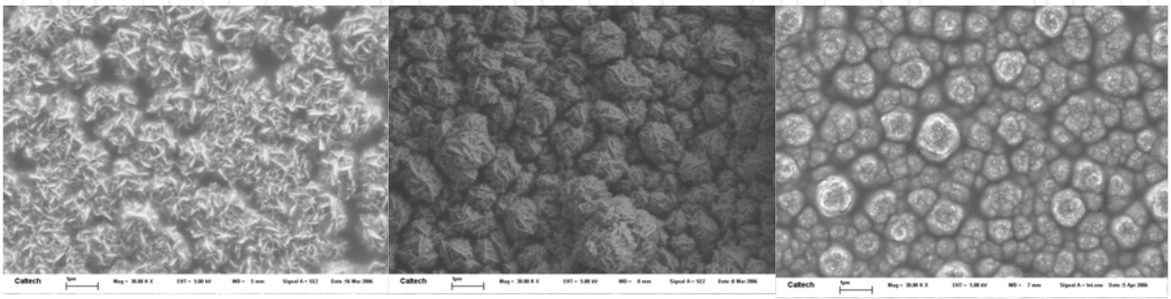

Figure 22. Magnified views of possible surface morphologies after platinization.

http://dx.doi.org/10.5772/55308

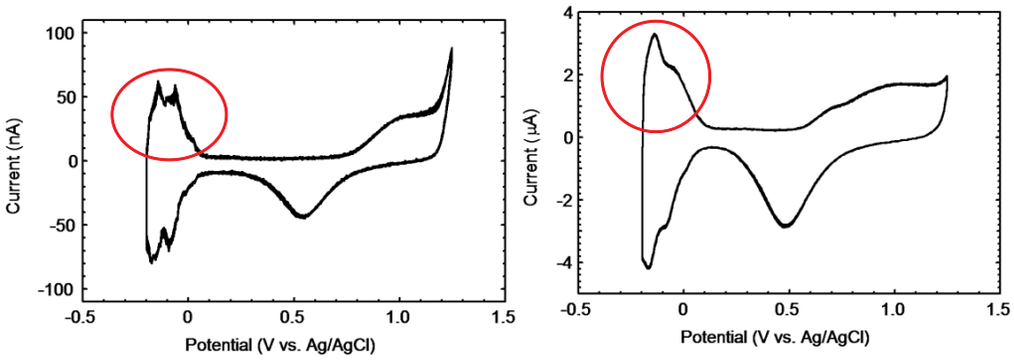

Figure 23. CVs showing more than 40-fold increase in electrode surface area from before plating (left) and after plating (right). The surface area is estimated by integrating the area under the peaks circled in red. Note change in scale of the ordinate. Scan rate: 100 mV/s. Electrolyte: O_2-free H_2SO_4 (N_2-bubbled).

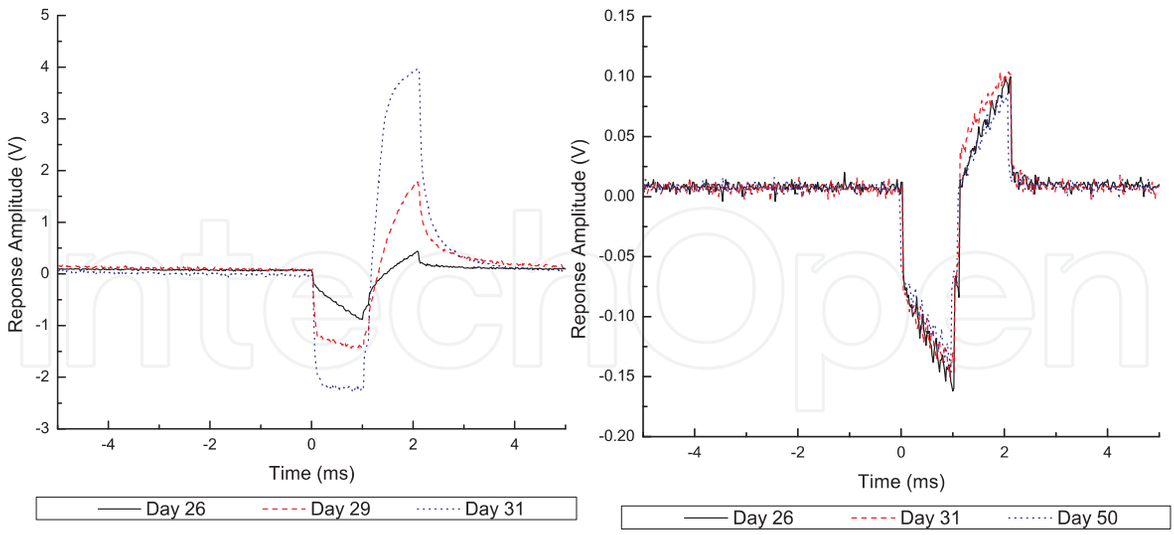

Figure 24. Voltage responses to a current pulse for (left) an unplated electrode, documenting the process of electrode failure, and (right) a plated electrode, showing steady responses throughout the 50 day test. Note response amplitudes for plated electrodes are far lower than those for the unplated electrode, as expected [27].

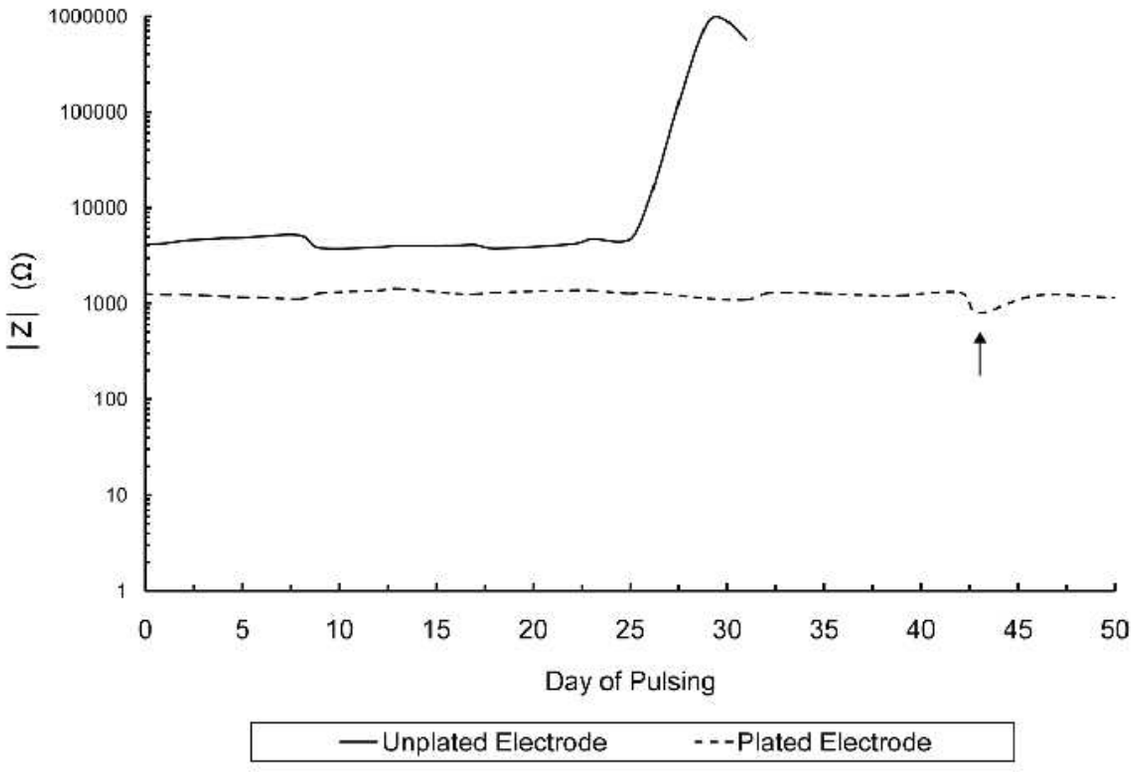

Figure 25. Magnitude of the electrochemical impedances at 1 kHz of an unplated and plated electrode over time. The unplated electrode showed a dramatic increase in impedance around day 30, at which time the test was stopped, whereas the plated electrode showed steady impedance through day 50. The arrow denotes a temporary dip in impedance due to CV scanning.

9. Chip-level integrated interconnect technology

9.1. Introduction

Despite our ability to fabricate such a large number of electrodes in such a small area, a significant impediment to future progress is the problem of how to package and interconnect these multielectrode arrays with foundry-fabricated ASICs, discrete components (e.g., chip capacitors, oscillators, diodes) and RF coils in a way that provides for high lead-count interconnects. A wafer-level process is cost prohibitive, as it is necessary to maximize the area of a wafer devoted to IC processing to keep costs low. Furthermore, current technologies for packaging would be far too tedious and low yield to apply to a 1000-electrode device. In order to achieve our goal of a 1000-electrode retinal prosthesis and a high-density spinal cord stimulation system, then, a new way of forming such a package so as to enable high-lead-count integration is necessary.

We have invented a way to place prefabricated chips, manufactured, for example, at a foundry, into the fabrication process of a parylene-based multielectrode array and/or RF coil, such that

http://dx.doi.org/10.5772/55308

all interconnections to the chip are made using standard photolithography and standard microfabrication techniques in a fully scalable manner [40]. This packaging scheme is known as the chip-level integrated interconnect (CL-I²) package. Figure 26 shows an overview of the fabrication process and how multiple chips could be joined together in this manner. A detailed discussion of the fabrication process, as adapted from [40], follows.

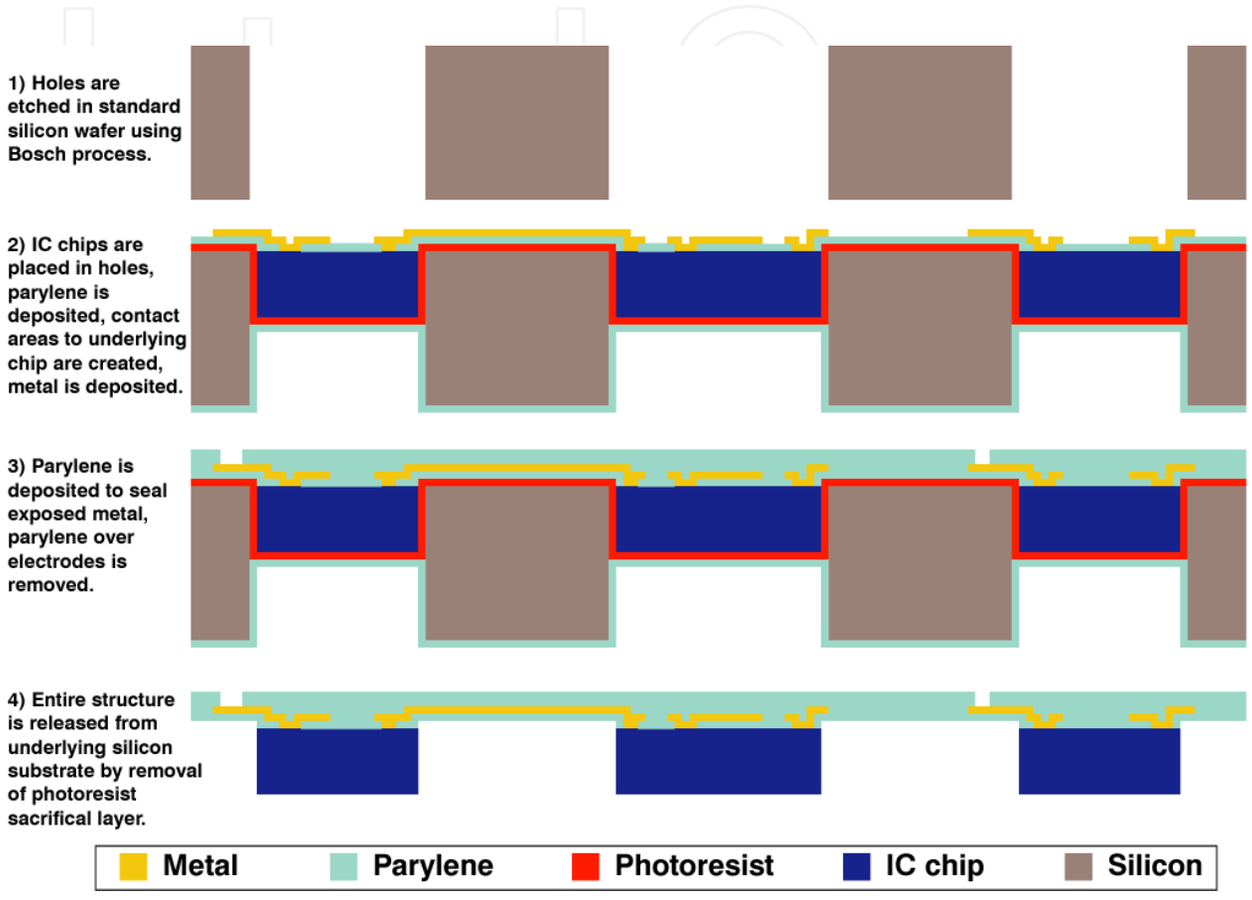

Figure 26. Overview of the CL-I² process. Multiple chip connections are possible.

9.2. Fabrication

Three MOSIS-fabricated ASICs, as well as seven chips fabricated to simulate them (with circuitry that facilitated testing), were used to demonstrate the CL-I² packaging technology. In order to fabricate the replicas of the MOSIS chips, these chips were imaged using a WYKO interferometer (Veeco Instruments Inc., Woodbury, NY, USA), and were found to have mean dimensions of 2.500 mm in length, 2.617 mm in width, and 254.2 μm in total thickness.

One hundred angstroms of chrome and 2000 Å of gold were e-beam evaporated on a 260 μm thick silicon wafer. Using a photoresist mask, the metal was wet etched to pattern pads of the same size and in the same locations as on the MOSIS-fabricated chips (approximately 70–100 × 100 μm² with a center-to-center pad spacing of approximately 200 μm), as well as a pattern of short circuits connecting these pads to nearby pads. After stripping the photoresist, a second

photoresist layer was spun on the wafer and patterned as a mask for a Bosch through-wafer etch in a PlasmaTherm SLR-770B deep reactive ion etching (DRIE) system (Unaxis Corporation, St. Petersburg, FL, USA). This etch defined the length, width, and thickness of the simulated chips as 2.49 mm, 2.61 mm, and 260 μm, respectively. Finally, the photoresist mask was removed from the individual chips. In this manner, chips comprising simple electrical shorts and intrinsic resistors were fabricated as our primary CL-I^2 package test structures (Figure 27.)

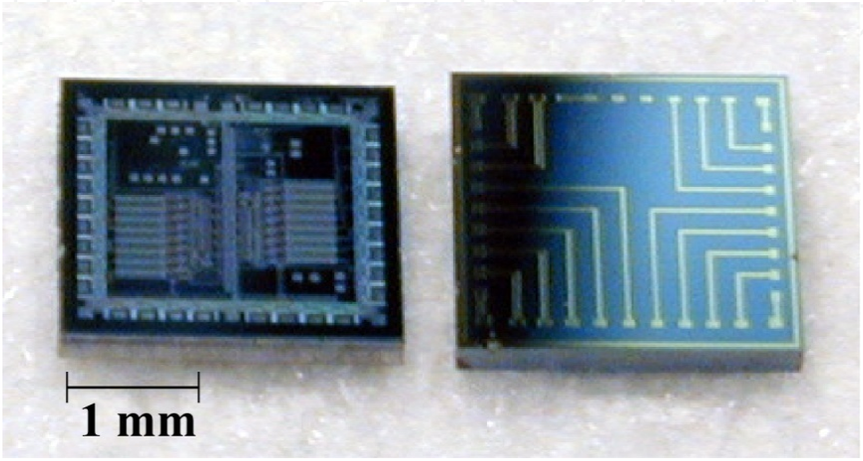

Figure 27. MOSIS ASIC (left) next to test chip (right).

The only properties of these prefabricated chips that had to be known before incorporation in the CL-I^2 process were their overall length, width, and thickness, and the dimensions and locations of the contact pads. Figure 28 gives a detailed CL-I^2 process flow. To begin, shallow alignment marks are etched into a standard 550 μm thick silicon wafer using a thin photoresist mask and an SF_6 plasma. 2.51 × 2.63 mm^2 holes are then patterned after alignment in a 10X reduction stepper in thick photoresist and an optional silicon dioxide mask. Through holes are then etched using the Bosch DRIE process. After photoresist and oxide removal, Nitto tape is placed on the frontside of the wafer. The chips are then self-aligned in the holes by inserting them from the backside (the Nitto tape enables frontside planarization whereas the lateral dimensions of the etched cavity determine lateral displacement), and they are sealed in place using several drops of sacrificial photoresist to cover the backside of the chip and to fill the gaps around it. A subsequent approximately 12 μm thick parylene C deposition in a PDS2010 mechanically anchors the chips in place from the backside. After removal of the frontside parylene by peeling off the Nitto tape, vertical displacements of the chips are measured using a stylus profilometer (Alphastep 200 and P-15, KLA-Tencor, San Jose, CA, USA).

The parylene-based flexible electrodes, or, in this implementation, contact pads for electrical testing, are then fabricated on this wafer as if it were a whole wafer with prefabricated integrated circuitry. First, a photoresist sacrificial layer is spun on the wafer and patterned to

http://dx.doi.org/10.5772/55308

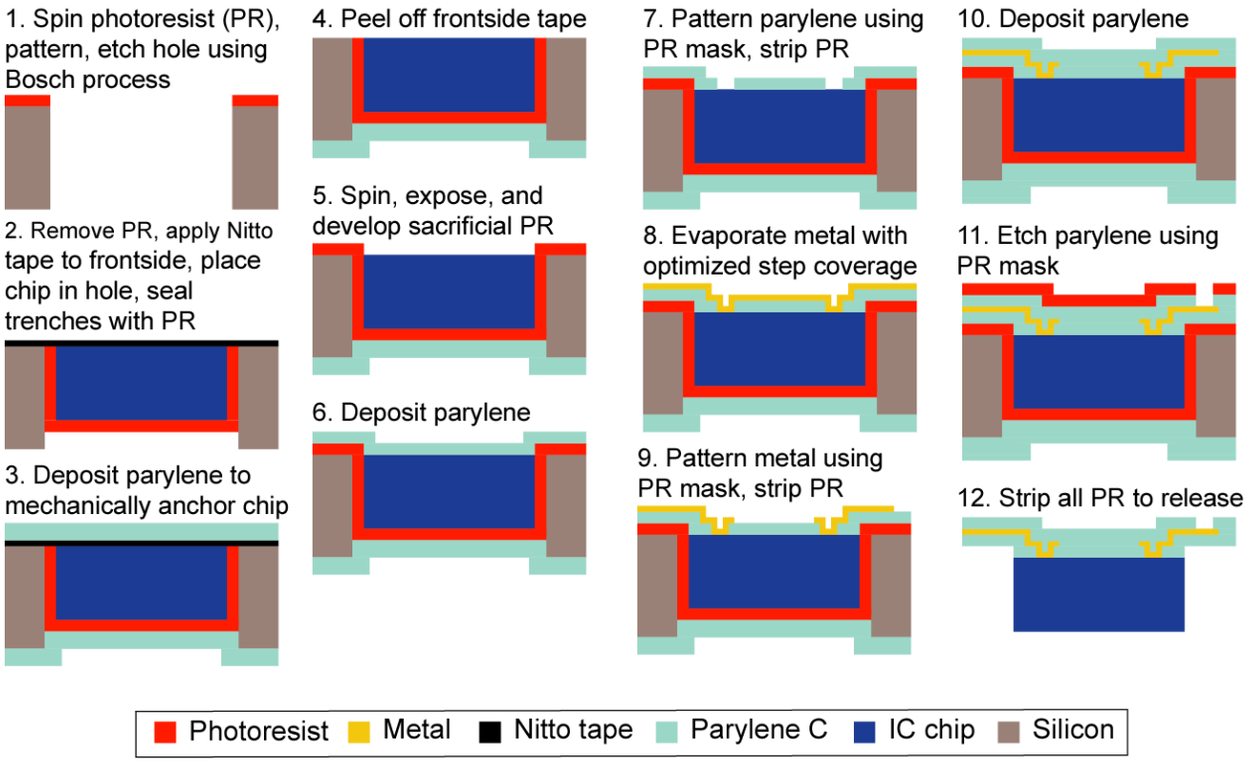

Figure 28. Detailed process flow for CL-I^2 package fabrication.

expose the chip's surface. After baking to remove excess solvent, approximately 3 μm of parylene C is deposited on the entire wafer. Photoresist is spun on the wafer, exposed in the 10X reduction stepper, and developed to pattern etch holes above the on-chip pads, similar to the vias in the dual metal-layer process. This pattern is transferred into the parylene using an O_2 plasma in an RIE system, exposing the metal of these on-chip pads. Two hundred angstroms of titanium and 2000 Å of gold are deposited in the e-beam evaporation system using optimized step coverage, and patterned (using a photoresist mask and wet etching) to define the remote contact pads and remote pad to on-chip pad interconnects. The top photoresist is stripped, and a second layer of approximately 10 μm of parylene C is deposited and patterned as before, but this time to open the remote pads/electrodes to enable electrical testing. Finally, all photoresist, including the sacrificial layer, is removed by soaking the wafer in acetone, releasing a flexible parylene skin with embedded interconnects to the packaged ASIC. The host wafer can be substituted in the process with a precisely machined substrate, and can be reused after this release step. It is also important to note that the ASIC or discrete component can be of any thickness, but generally the thickness should be less than that of the host wafer or machined substrate, and it can have parylene or any hermetic coating deposited on it *a priori*, provided that the chip contacts can be opened using microfabrication techniques before the interconnect metal is laid down and patterned (Figure 28 steps 8 and 9). Thus, this technology combines the best aspects of chip-level packaging, in which every surface of the prefabricated chip can

be manipulated or coated beforehand, and wafer-level packaging, in that photolithography and microfabrication can be performed on the surface after such chip-level techniques.

9.3. Integration testing results

We successfully performed photolithography on ten prefabricated stand-alone chips using this paradigm: seven test chips (three conformally coated in parylene *a priori*) and three MOSIS-fabricated chips (one coated in parylene *a priori*). A MOSIS chip anchored in place in the host substrate is shown centrally in Figure 29 with the host wafer shown on the perimeter. As is expected, minimizing vertical displacement of the ASIC from the wafer surface is crucial for further photolithography steps. Figure 30 gives typical surface profiles of all ten chips with respect to the surrounding host wafer, and indicates that for most chips, this vertical displacement was less than 5 μm after removal of the frontside Nitto tape. Photolithography on the somewhat anomalous test chips 2 and 7, however, was also successful.

The accurate horizontal alignment of the perimeter interconnects to the embedded chips is shown in Figure 31, with Figure 32 giving a detailed micrograph of a single interconnect for both the test chip (a) and the MOSIS chip (b). By design, the chips should be self-aligned to within 10 μm of lateral displacement; some chips were aligned far better than this, however others were misaligned worse than this. With tighter tolerances on the cavity sidewalls, or with chip-alignment lithographic equipment, this alignment error could be improved. The embedded chip with remote contact pads is shown in Figure 33, and Figure 34 depicts the flexibility of this package. Functional contacts to the chips were verified as described in [40].

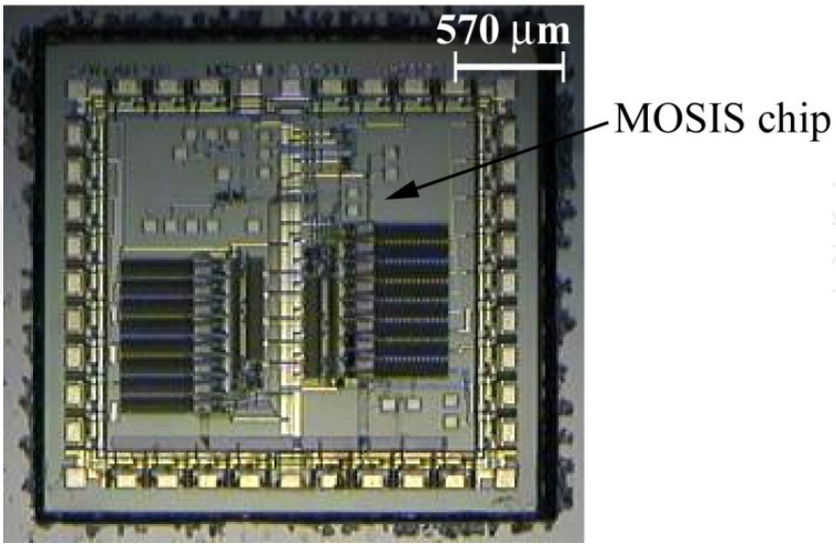

Figure 29. MOSIS chip (center) shown anchored in host silicon substrate (perimeter).

http://dx.doi.org/10.5772/55308

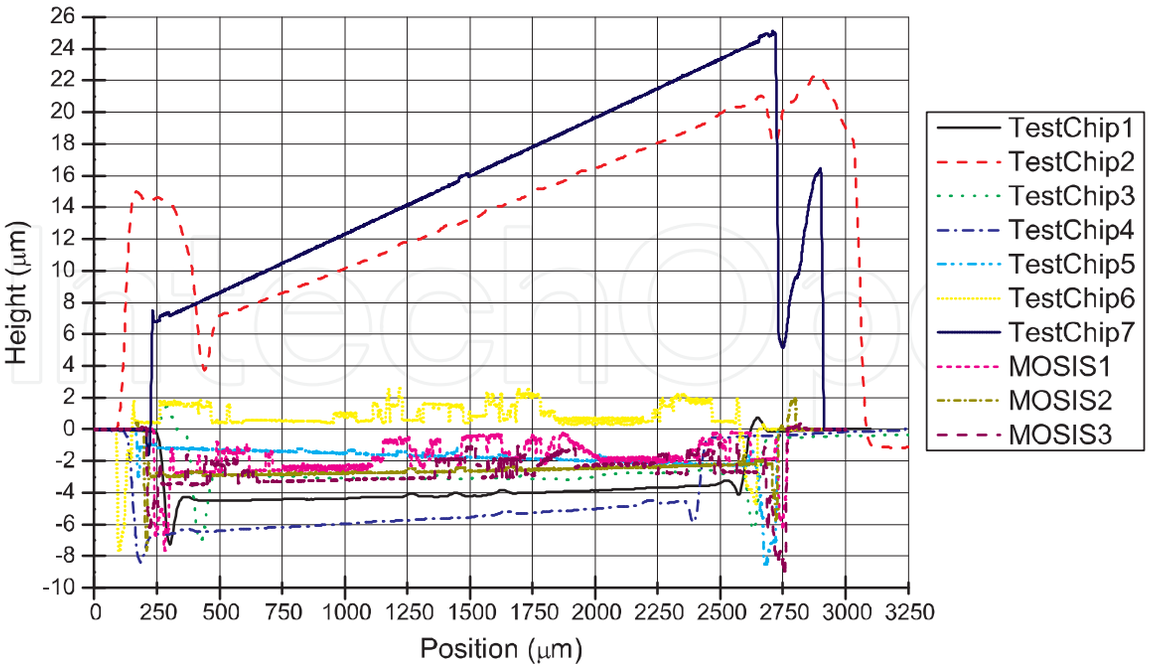

Figure 30. Typical single-axis vertical displacements of all 10 chips after mechanical anchoring in the host wafer (Figure 28, step 4), where the top surface of the wafer corresponds to 0 μm.

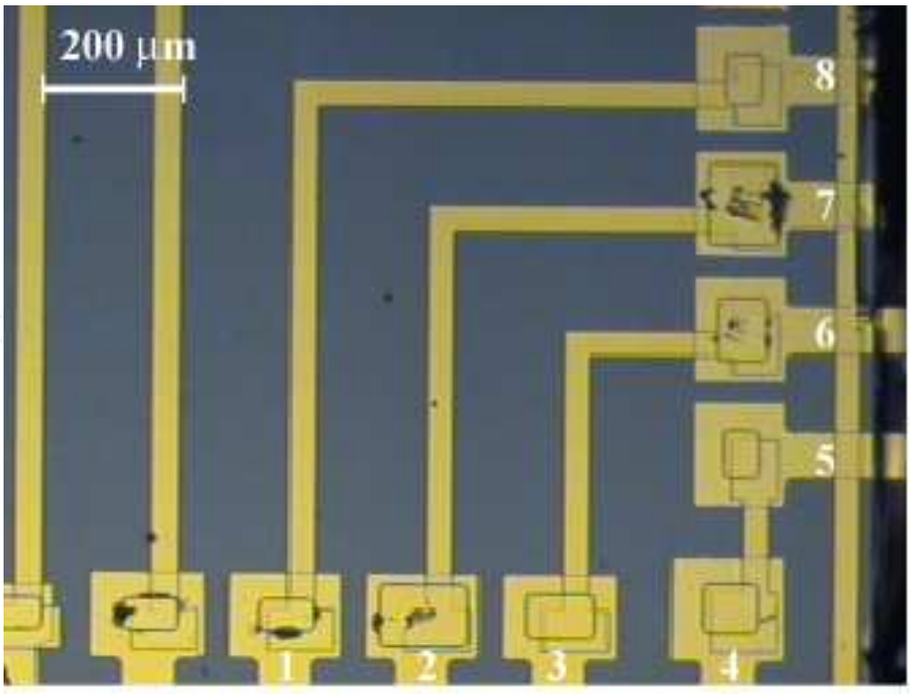

Figure 31. Embedded chip with fabricated perimeter interconnects (numbered traces connect to numbered remote pads shown in Figure 33).

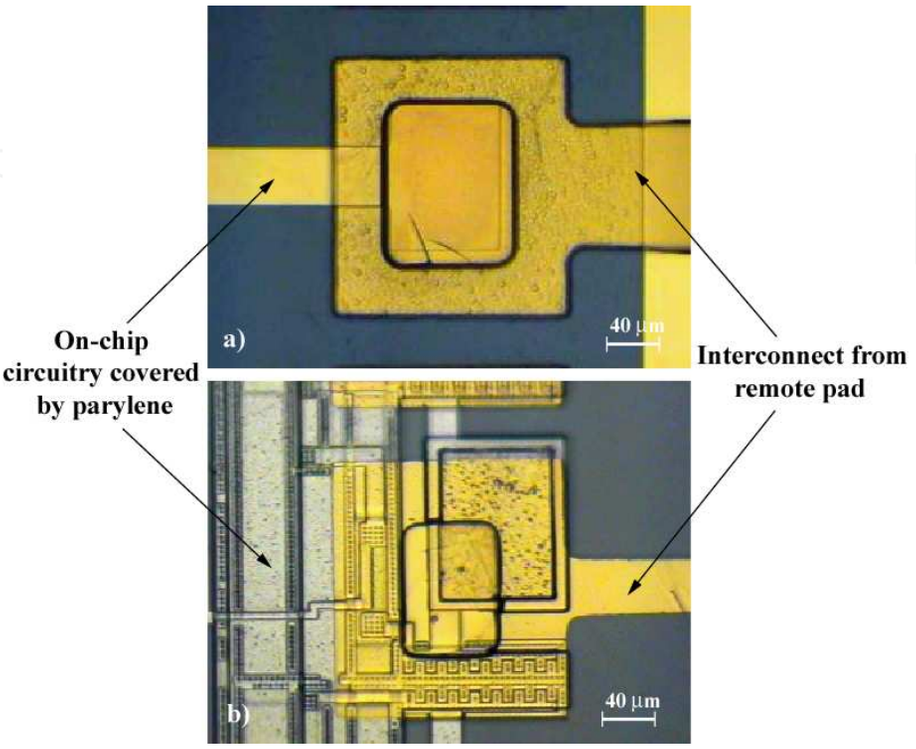

Figure 32. (a) Example of <10 μm lateral misalignment of a test chip; (b) Example of >10 μm lateral misalignment of a MOSIS chip.

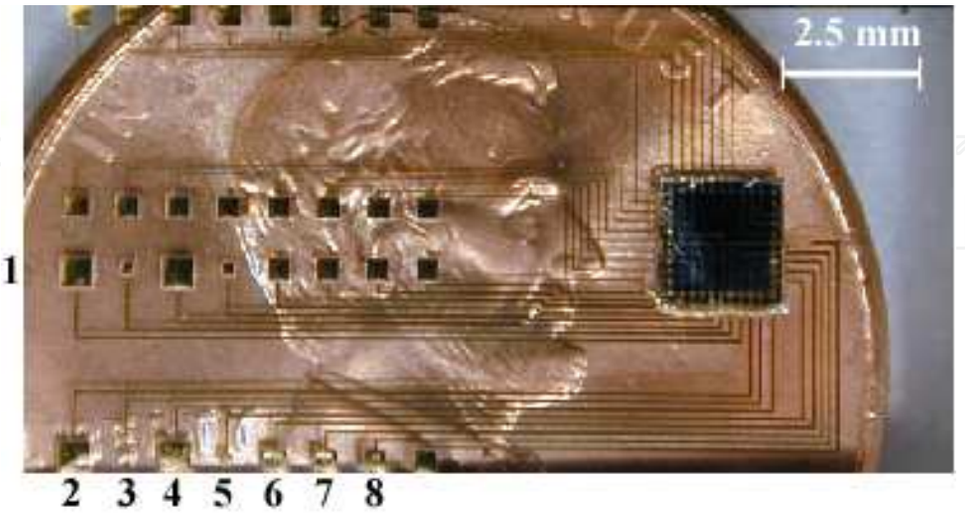

Figure 33. A CL-I^2 packaged chip shown resting on a penny.

http://dx.doi.org/10.5772/55308

Figure 34. Demonstrates flexibility of CL-I^2 package. Chip can be seen underlying overlying parylene "skin."

9.4. Discussion

It should be stressed that the lead-count and interconnect density limitations for this technology stem only from the limitations of the microfabrication and photolithography equipment used to fabricate the CL-I^2 package, and, in particular, to pattern the first parylene etch (Figure 28, step 7). All interconnects to the chip are fabricated simultaneously during the metal deposition step, and depend on optimal step coverage of the parylene sidewall (aided in part by the slightly isotropic nature of the O_2 plasma etch of parylene [47]). The CL-I^2 process thus avoids the use of tedious and comparatively low-density ball-wedge [38] or wire bonding.

Our method of incorporating discrete modules into a MEMS process is far more cost-effective when compared with full-wafer IC processing and MEMS integration [51], because valuable space on the wafer is not wasted during the IC fabrication step. Furthermore, in comparison to other ASIC integration attempts [51-53], this packaging scheme is superior for biodevices because it takes advantage of parylene's low water-absorption [54] and highly conformal pinhole-free deposition, and because the package is both flexible and biocompatible. Among the feasible uses for this technology is the interconnection of chips, devices such as other CMOS-compatible MEMS, as well as discrete components such as chip capacitors, fabricated using different materials and processes, to make large conglomerate circuits for neural prostheses and for other applications. This technology is capable of increasing the previously projected number of I/O interconnects available in 2010 significantly, while using lead-free, biocompatible materials. Fabrication is not limited to the use of parylene as either the backside anchoring material or as the frontside electrode insulation material, although, because of its superior electrical, mechanical, and water permeability properties when compared with other polymers, we believe parylene will ultimately prove to be the best choice for monolithic high-density neural prosthetics. It is interesting to note that another research group has, after our

original publications [40, 56, 57], explored an integration technique in polyimide very similar to ours, with interconnect density motivations much akin to our own [58]. We have recently demonstrated a fully integrated parylene-based single-channel neural stimulator [59]. *In vitro* measurements demonstrated the ability to generate 7 V pulses of 500 μs pulse width from a wireless transmitter 4 mm away. Preliminary evidence from animal implantation studies has shown these are mechanically reliable under surgical conditions.

10. Conclusions and future work

BioMEMS, an emerging field in which MEMS are designed, fabricated, and utilized to interface with and examine biological systems, is a discipline replete with incredible possibilities, but also one that is fraught with potential pitfalls. This is no more true than in the case of implantable microelectronics, where applications abound because of the near perfect match in the sizes of the functional components of the body, namely cells and neurons, and the technologies possible using microfabrication techniques. Materials must be carefully selected such that they are biocompatible with the body, while still enabling maximal functionality to be delivered to the patient, requirements that are often competing in nature. In this vein, the microtechnologies necessary for parylene-based flexible microelectrode technologies have been presented. All evidence thus far points to the fact that such parylene-based technologies are likely an ideal option for implantable neuroprostheses and microdevices.

It should be stressed that these technologies are not limited to use in retinal and spinal cord prostheses. In fact, the ability of our flexible arrays to conform to the geometries of interest in the human body enables them to be used in a variety of locations heretofore previously inaccessible with such high precision. Such locations include the surfaces of the cerebral cortex, another area of interest from both a scientific and treatment point of view due to such neurological problems as stroke, epilepsy, and memory loss. Areas of other interest include peripheral nerve and muscle. It is also possible to embed sensors in such arrays, as has recently been demonstrated [60], to assess mechanical forces placed on the tissues of interest by our arrays as well as to detect extrinsic pressures, such as those within the eye or within blood vessels.

Understandably, there is a public reticence to the implementation of such technologies in the human body. While such apprehension is not a recent phenomenon, the burgeoning era of computerized special effects in television and cinema has helped fuel the fear that the blending of “man” and “machine” can have devastating consequences. What is missed in such intimations is that, in the hands of ethical doctors, engineers, and other scientists, such consequences are extremely remote. But it is not about the inventors of these technologies, and it should never be about personal glory. All of that slips away the moment one talks to a person who has devoted their life to be a pioneer in the field by volunteering to be a test subject of such devices for the benefit of mankind. In such conversations, one realizes the full potential of this technology. Investigation into these devices not only has the possibility to positively affect the lives of such people, by enabling them to “walk” or “see” again, but it transcends all that by bringing about in all involved a sense of camaraderie. Indeed, the selfless motivation of such

http://dx.doi.org/10.5772/55308

individuals who devote their most precious commodity, their body, to such studies, more than anything else highlights our very humanity. It shows that, despite the need for such technological innovation, it is only by working together and for one another that we, as a people, can break the bonds of human disease.

Author details

Damien C. Rodger[1], Wen Li[2], James D. Weiland[1], Mark S. Humayun[1] and Yu-Chong Tai[3]

1 University of Southern California, Los Angeles, CA, USA

2 Michigan State University, East Lansing, MI, USA

3 California Institute of Technology, Pasadena, CA, USA

References

[1] The Eye Diseases Prevalence Research Group, "Prevalence of age-related macular degeneration in the United States," *Arch Ophthalmol,* vol. 122, pp. 564-572, April 1 2004.

[2] G. Fishman, V. Vasquez, M. Fishman, and D. Berger, "Visual loss and foveal lesions in Usher's syndrome," *Br J Ophthalmol,* vol. 63, pp. 484-488, Jul 1 1979.

[3] B. W. Jones, C. B. Watt, J. M. Frederick, W. Baehr, C.-K. Chen, E. M. Levine, A. H. Milam, M. M. Lavail, and R. E. Marc, "Retinal remodeling triggered by photoreceptor degenerations," *The Journal of Comparative Neurology,* vol. 464, pp. 1-16, 2003.

[4] E. Margalit and S. R. Sadda, "Retinal and Optic Nerve Diseases," *Artificial Organs,* vol. 27, pp. 963-974, 2003.

[5] A. Santos, M. S. Humayun, E. de Juan, Jr., R. J. Greenburg, M. J. Marsh, I. B. Klock, and A. H. Milam, "Preservation of the inner retina in retinitis pigmentosa. A morphometric analysis," *Arch Ophthalmol,* vol. 115, pp. 511-515, April 1, 1997 1997.

[6] R. E. MacLaren, R. A. Pearson, A. MacNeil, R. H. Douglas, T. E. Salt, M. Akimoto, A. Swaroop, J. C. Sowden, and R. R. Ali, "Retinal repair by transplantation of photoreceptor precursors," *Nature,* vol. 444, pp. 203-207, 2006.

[7] M. Humayun, R. Propst, E. de Juan, Jr., K. McCormick, and D. Hickingbotham, "Bipolar surface electrical stimulation of the vertebrate retina," *Arch Ophthalmol,* vol. 112, pp. 110-116, Jan 1 1994.

[8] M. S. Humayun, E. de Juan, Jr., G. Dagnelie, R. J. Greenberg, R. H. Propst, and D. H. Phillips, "Visual perception elicited by electrical stimulation of retina in blind humans," *Arch Ophthalmol,* vol. 114, pp. 40-46, January 1, 1996 1996.

[9] M. A. Schiefer and W. M. Grill, "Sites of Neuronal Excitation by Epiretinal Electrical Stimulation," *IEEE Transactions on Neural Systems and Rehabilitation Engineering,* vol. 14, pp. 5-13, 2006.

[10] A. Y. Chow and V. Y. Chow, "Subretinal electrical stimulation of the rabbit retina," *Neuroscience Letters,* vol. 225, pp. 13-16, Mar 28 1997.

[11] C. Veraart, M. C. Wanet-Defalque, B. Gerard, A. Vanlierde, and J. Delbeke, "Pattern recognition with the optic nerve visual prosthesis," *Artificial Organs,* vol. 27, pp. 996-1004, Nov 2003.

[12] E. M. Schmidt, M. J. Bak, F. T. Hambrecht, C. V. Kufta, D. K. ORourke, and P. Vallabhanath, "Feasibility of a visual prosthesis for the blind based on intracortical microstimulation of the visual cortex," *Brain,* vol. 119, pp. 507-522, Apr 1996.

[13] E. M. Maynard, "Visual prostheses," *Annual Review of Biomedical Engineering,* vol. 3, pp. 145-168, 2001.

[14] J. S. Pezaris and R. C. Reid, "Demonstration of artificial visual percepts generated through thalamic microstimulation," *PNAS,* vol. 104, pp. 7670-7675, May 1, 2007 2007.

[15] M. S. Humayun, J. D. Weiland, G. Y. Fujii, R. Greenberg, R. Williamson, J. Little, B. Mech, V. Cimmarusti, G. Van Boemel, and G. Dagnelie, "Visual perception in a blind subject with a chronic microelectronic retinal prosthesis," *Vision Research,* vol. 43, pp. 2573-2581, Nov. 2003.

[16] M. S. Humayun, R. Freda, I. Fine, A. Roy, G. Fujii, R. J. Greenberg, J. Little, B. Mech, J. D. Weiland, and E. de Juan, "Implanted intraocular retinal prosthesis in six blind subjects," *Investigative Ophthalmology & Visual Science,* vol. 46, p. 1144, 2005.

[17] B. S. Wilson, C. C. Finley, D. T. Lawson, R. D. Wolford, D. K. Eddington, and W. M. Rabinowitz, "Better speech recognition with cochlear implants," *Nature,* vol. 352, pp. 236-8, Jul 18 1991.

[18] J. D. Weiland, W. Liu, and M. S. Humayun, "Retinal prosthesis," *Annual Review of Biomedical Engineering,* vol. 7, pp. 361-401, 2005.

[19] C. J. Lee, J. A. Vroom, H. A. Fishman, and S. F. Bent, "Determination of human lens capsule permeability and its feasibility as a replacement for Bruch's membrane," *Biomaterials,* vol. 27, pp. 1670-8, Mar 2006.

[20] L. J. Noble and J. R. Wrathall, "Correlative Analyses of Lesion Development and Functional Status after Graded Spinal-Cord Contusive Injuries in the Rat," *Experimental Neurology,* vol. 103, pp. 34-40, Jan 1989.

[21] K. Kurohane, A. Tominaga, K. Sato, J. R. North, Y. Namba, and N. Oku, "Photodynamic therapy targeted to tumor-induced angiogenic vessels.," *Cancer Lett,* vol. 167, pp. 49-56, Jun 2001.

[22] K. E. Krishnan L, Jewell WR, "Immediate effect of irradiation on microvasculature.," *Int J Radiat Oncol Biol Phys,* vol. 15, pp. 1147-1450, Jul 1988.

[23] J. W. Little, J. F. Ditunno, S. A. Stiens, and R. M. Harris, "Incomplete spinal cord injury: Neuronal mechanisms of motor recovery and hyperreflexia," *Archives of Physical Medicine and Rehabilitation,* vol. 80, pp. 587-599, May 1999.

[24] J. H. Burridge, P. N. Taylor, S. A. Hagan, D. E. Wood, and I. D. Swain, "The effects of common peroneal stimulation on the effort and speed of walking: a randomized controlled trial with chronic hemiplegic patients," *Clinical Rehabilitation,* vol. 11, pp. 201-210, Aug 1997.

[25] J. Rozman, R. Acimovicjanezic, I. Tekavcic, M. Kljajic, and M. Trlep, "Implantable Stimulator for Selective Stimulation of the Common Peroneal Nerve - a Preliminary-Report," *Journal of Medical Engineering & Technology,* vol. 18, pp. 47-53, Mar-Apr 1994.

[26] P. Taylor, J. Burridge, A. Dunkerley, D. Wood, J. Norton, C. Singleton, and I. Swain, "Clinical audit of 5 years provision of the Odstock dropped foot stimulator," *Artificial Organs,* vol. 23, pp. 440-442, May 1999.

[27] K. W. Horch and G. S. Dhillon, *Neuroprosthetics theory and practice*. River Edge, N.J.: World Scientific, 2004.

[28] R. Brissot, P. Gallien, M. P. Le Bot, A. Beaubras, D. Laisne, J. Beillot, and J. Dassonville, "Clinical experience with functional electrical stimulation-assisted gait with parastep in spinal cord-injured patients," *Spine,* vol. 25, pp. 501-508, Feb 15 2000.

[29] D. Graupe and K. H. Kohn, "Functional neuromuscular stimulator for short-distance ambulation by certain thoracic-level spinal-cord-injured paraplegics," *Surgical Neurology,* vol. 50, pp. 202-207, Sep 1998.

[30] E. Roederer, N. H. Goldberg, and M. J. Cohen, "Modification of retrograde degeneration in transected spinal axons of the lamprey by applied DC current," *J. Neurosci.,* vol. 3, pp. 153-160, January 1, 1983 1983.

[31] C. C. Stichel and H. W. Muller, "Experimental strategies to promote axonal regeneration after traumatic central nervous system injury," *Progress in Neurobiology,* vol. 56, pp. 119-148, 1998.

[32] S. A. Maguire AM, *Radiation retinopathy. In: Retina*. St. Louis: Mosby-Year book., 1994.

[33] M. Szwarc, "Some Remarks on the CH2=Benzene=CH2 Molecule," *Discussions of the Faraday Society,* vol. 2, pp. 46-49, 1947.

[34] W. F. Gorham, "A New General Synthetic Method for Preparation of Linear Poly-P-Xylylenes," *Journal of Polymer Science Part A-1: Polymer Chemistry,* vol. 4, pp. 3027-3039, 1966.

[35] L. Wolgemuth, "Crystal-Clear Coating Covers Components," *Medical Design,* vol. 6, pp. 48-51, December 1 2006.

[36] "New SCS Parylene HT Conformal Coating Ideal For High-Temperature Applications." vol. 2007: Specialty Coating Systems.

[37] "Reliable protection for advanced electronics." vol. 2007: Specialty Coating Systems.

[38] T. Stieglitz, W. Haberer, C. Lau, and M. Goertz, "Development of an inductively coupled epiretinal vision prosthesis," in *Int. IEEE Eng. in Med. and Biol. Soc. Meet.*, San Francisco, CA, USA, 2004, pp. 4178-4181 Vol.6.

[39] A. C. Hoogerwerf and K. D. Wise, "A three-dimensional microelectrode array for chronic neural recording," *IEEE Transactions on Biomedical Engineering,* vol. 41, pp. 1136-1146, 1994.

[40] D. C. Rodger, J. D. Weiland, M. S. Humayun, and Y.-C. Tai, "Scalable high lead-count parylene package for retinal prostheses," *Sensors and Actuators B: Chemical,* vol. 117, pp. 107-114, 2006.

[41] W. Li, D. C. Rodger, E. Meng, J. D. Weiland, M. S. Humayun, and Y.-C. Tai, "Flexible Parylene Packaged Intraocular Coil for Retinal Prostheses," in *Int. IEEE-EMBS Microtech. in Med. and Bio. Meet.*, Okinawa, Japan, 2006, pp. 105-108.

[42] P. J. Chen, D. C. Rodger, M. S. Humayun, and Y. C. Tai, "Unpowered spiral-tube parylene pressure sensor for intraocular pressure sensing," *Sensors and Actuators a-Physical,* vol. 127, pp. 276-282, Mar 13 2006.

[43] P. J. Chen, D. C. Rodger, E. M. Meng, M. S. Humayun, and Y. C. Tai, "Surface-micromachined parylene dual valves for on-chip unpowered microflow regulation," *Journal of Microelectromechanical Systems,* vol. 16, pp. 223-231, Apr 2007.

[44] E. Meng, P.-J. Chen, D. Rodger, Y.-C. Tai, and M. Humayun, "Implantable parylene MEMS for glaucoma therapy," in *Int. IEEE-EMBS Microtech. in Med. and Bio. Meet.*, Oahu, HI, USA, 2005, pp. 116-119.

[45] A. K. Ahuja, M. R. Behrend, M. Kuroda, M. S. Humayun, and J. D. Weiland, "Spatial Response Properties of Electrically Stimulated Retina," *Invest. Ophthalmol. Vis. Sci.,* vol. 48, p. 4444, May 10 2007.

[46] A. P. Chandran, K. Oda, H. Shibasaki, and M. Pisharodi, "Spinal somatosensory evoked potentials in mice and their developmental changes," *Brain Dev,* vol. 16, pp. 44-51, Jan-Feb 1994.

[47] E. Meng and Y.-C. Tai, "Parylene etching techniques for microfluidics and bio-MEMS," in *IEEE Int. Conf. on MEMS*, Miami, FL, USA, 2005, pp. 568-571.

[48] C. A. Curcio and K. A. Allen, "Topography of Ganglion-Cells in Human Retina," *Journal of Comparative Neurology*, vol. 300, pp. 5-25, Oct 1990.

[49] J. J. Whalen, J. D. Weiland, and P. C. Searson, "Electrochemical Deposition of Platinum from Aqueous Ammonium Hexachloroplatinate Solution," *Journal of The Electrochemical Society*, vol. 152, pp. C738-C743, 2005.

[50] S. B. Brummer and M. J. Turner, "Electrical Stimulation with Pt Electrodes: I-A Method for Determination of "real" electrode Areas," *IEEE Transactions on Biomedical Engineering*, vol. 24, pp. 436-439, 1977.

[51] Y. Xu, Y.-C. Tai, A. Huang, and C.-M. Ho, "IC-integrated flexible shear-stress sensor skin," *Microelectromechanical Systems, Journal of*, vol. 12, pp. 740-747, 2003.

[52] J. T. Butler, V. M. Bright, and J. H. Comtois, "Advanced multichip module packaging of microelectromechanical systems," in *Int. Conf. on Solid-State Sensors and Actuators*, Chicago, IL, USA, 1997, pp. 261-264.

[53] W. Daum, W. E. Burdick, and R. A. Fillion, "Overlay high-density interconnect: a chips-first multichip module technology," *Computer*, vol. 26, pp. 23-29, 1993.

[54] J. J. Licari and L. A. Hughes, *Handbook of polymer coatings for electronics : chemistry, technology, and applications*, 2nd ed. Park Ridge, N.J., U.S.A.: Noyes Publications, 1990.

[55] R. R. Tummala, *Fundamentals of microsystems packaging*. New York: McGraw-Hill, 2001.

[56] D. C. Rodger and Y. C. Tai, "Microelectronic packaging for retinal prostheses," *IEEE Engineering in Medicine and Biology Magazine*, vol. 24, pp. 52-57, Sep-Oct 2005.

[57] D. C. Rodger, J. D. Weiland, M. S. Humayun, and Y.-C. Tai, "Scalable flexible chip-level parylene package for high lead count retinal prostheses," in *Int. Conf. Solid-State Sensors, Actuators and Microsystems*, Seoul, Korea, 2005, pp. 1973-1976.

[58] H. Sharifi, T. Y. Choi, and S. Mohammadi, "Self-aligned wafer-level integration technology with high-density interconnects and embedded passives," *IEEE Transactions on Advanced Packaging*, vol. 30, pp. 11-18, Feb 2007.

[59] W. Li, D. C. Rodger, A. Pinto, E. Meng, J. D. Weiland, M. S. Humayun, and Y.-C. Tai, "Parylene-based integrated wireless single-channel neurostimulator," *Sensors and Actuators A: Physical*, vol. 166, pp. 193-200.

[60] B. J. Kim, C. A. Gutierrez, G. A. Gerhardt, and E. Meng, "Parylene-based electrochemical-MEMS force sensor array for assessing neural probe insertion mechanics," in *Micro Electro Mechanical Systems (MEMS), 2012 IEEE 25th International Conference on*, pp. 124-127.

IntechOpen